united nations
educational, scientific
and cultural
organization

international atomic
energy agency

the
abdus salam
international centre for theoretical physics

Winter College on Optics and Photonics
7 - 25 February 2000

1218-24

"Chaos & Encrytion & Coherence Modulation"
(Reprints)

W.T. RHODES
Georgia Institute of Technology
USA

Communicating
with Synchronized Hyperchaos.

V. S. Udaltsov, J. P. Goedgebuer and W. T. Rhodes

GTL-CNRS TELECOM Georgia Tech Lorraine, 2, rue Marconi 57070 Metz, France

Abstract

Recent theoretical studies and experimental demonstrations have shown the possibility of using high-dimensional chaos for the encryption of message signals in wideband communication systems. Chaos is generated by delayed-feedback nonlinear systems, which feature hyperchaotic (i.e., of high dimensionality) dynamics. Essentially identical chaos generators in transmitter and receiver pair can be synchronized in such a way that the encrypted signal can be determined, so long as the transmitted signal is extracted at the transmitter and injected at the receiver at the suitable point in the generators.

Introduction

Current methods for communicating message signals on noise-like chaotic carriers rely on two general approaches. The first, due to Ott, Grebogi, and Yorke (*1*), utilizes what has been referred to as controlled chaos. The dynamics of a chaotic electronic oscillator are made to follow prescribed orbits in the attractor through the addition of small perturbations, thereby allowing a message to be encoded in the chaotic waveform. A different method, developed by Pecora and Carroll (*2*) and later by Cuomo and Oppenheim (*3*), is based on what has been called synchronized chaos. A chaotic signal produced by a circuit at the transmitter is transmitted to an identical circuit at the receiver, where it produces a fully synchronized chaotic output. Information is transmitted by adding a small-amplitude message signal to a large chaotic carrier, the latter effectively hiding the former. The message is extracted at the receiver by subtracting the chaos created in the receiver from the transmitted chaos-plus-message signal.

As developed thus far, these two methods do not appear adequate for application to commercial telecommunication systems. First, the bandwidth of electronic circuits for chaotic signal generation is relatively low, typically below a megahertz. Second, and of much greater fundamental importance, only low-dimensional attractors (e.g., Chua's attractor, which has a single Lyapunov exponent) have been successfully employed (*4*). The chaos thus produced features low complexity, and an eavesdropper can decrypt the signal by using conventional signal processing techniques (*5*). Another chaos synchronization method introduced by Volkovskii and Rul'kov (*6*) was also used for ring electronic circuits, but the method was demonstrated to extremly low dimensionality chaos. For adequate security, high-dimensional chaos must be used.

It has recently been noted that both the low bandwidth and the low complexity limitations can be overcome through the use of lasers in time-delayed-feedback nonlinear system configurations. The bandwidth of such systems, limited ultimately by laser processes, is extremely high, potentially in the 100 GHz range. Furthermore, such systems produce chaos of high dimensionality—so-called hyperchaos—that can much more effectively mask message signals. Because of their different nature, the laser-based systems require different means for synchronization of transmitter and receiver than do those noted in the opening paragraph.

Two groups have conducted research on such laser-based systems. In 1998, Van Wiggeren and Roy demonstrated the transmission of 126 Mbits/s digital message signals

using a chaotic laser-oscillator system (*7*). Their transmitter consisted of a delayed feedback laser made from an erbium-doped fiber amplifier (EDFA). The receiver was formed by an open-loop EDFA and a fiber delay line effectively identical to that used in the transmitter. Identical configurations ensured that the receiver could be synchronized by injection of the chaotic signal received from the transmitter. Their system exhibited high-dimensional dynamics, of order 10 or greater (*8*), allowing secure masking of message information.

Also in 1998, our group demonstrated use of a wavelength-tunable laser diode in a nonlinear delayed feedback loop to generate a laser output that was chaotic in wavelength (*9*, *10*). The noise-like wavelength fluctuations were used to mask message information transmitted to a receiver. The receiver was again a precise replica of the transmitter, except that the feedback loop was open and fed directly with the signal from the transmitter. Through chaos-synchronization processes, the signal in the receiver locked to the hyperchaotic signal produced by the transmitter, and the message signal was recovered by subtraction of the chaos produced by the receiver from the transmitted chaos-encrypted signal. The dynamics of this particular system were indeed of high dimensionality, of order $5 \cdot 10^2$. Such high-dimensional chaos is common to time-delayed feedback systems of any kind.

These two laser-based systems, both of which rely on similar physical principles, appear to be the only effective systems reported so far demonstrating the possibility of using synchronized high-dimensional chaos to transmit information.

In discussions about such systems, challenging questions are frequently asked: "Is it still possible to synchronize the receiver when the amplitude of the message signal is high?" "How critically must transmitter and receiver parameters be matched to assure chaos synchronization?" "Is it always possible to recover directly the message at the receiver without using some additional processing?" And so forth. This article is intended to address such questions in a comprehensive way. The questions are of fundamental importance not only to the hyperchaotic laser systems noted above but also to many other systems — biological, chemical, electrical, mechanical (*11*) — characterized by nonlinear delayed-feedback chaos. They are addressed through consideration of the difference-differential equations that describe the dynamics of the chaos generation in transmitter and receiver.

Analysis

A system representative of those of concern is shown in Fig.1. It consists of a source, a nonlinear element, an ideal detector, a first-order low-pass filter with a time constant τ, and a feedback loop with a delay time T. For simplicity all gain in the system is associated with the detector. The dynamical state of such a system is governed by a well-known difference-differential equation, known as Ikeda's equation (*12*), which has the form

$$v(t) + \tau \frac{dv(t)}{dt} = \beta \cdot F[v(t-T)], \tag{1}$$

where $v(t)$ represents the chaotic signal in the system, $F(v)$ is a nonlinear function featuring one or more extrema, and β is a gain factor known as the bifurcation parameter. An alternative form of this equation that maps directly onto the system shown in Fig. 1 is given by

$$v(t)+\tau\frac{dv(t)}{dt}=\beta\cdot NL\{f[v(t-T)]\}, \tag{2}$$

where f(.) is associated with the source and where NL{.} represents the nonlinearity introduced by the separate nonlinear element. Equation (1) has been extensively investigated, especially for the case when the nonlinear function is quadratic, i.e., $F(v) = \gamma v^2$ (yielding the so-called logistic map), or when $F(v) = \sin^2(v)$.

Systems described by difference-differential equations of the form Eqs. (1) and (2) can produce chaos of very high dimensionality when $T >> \tau$. For example, when $F(v) = \sin^2(v)$, the dimension d of the system is given approximately by $d = 0.4\beta T/\tau$ (the corresponding number of zero or positive Lyapunov exponents is approximately equal to $d/2$), the complexity increasing with the ratio T/τ and with the bifurcation parameter β. For β greater than approximately 15, the chaos generated has the characteristics of a Gaussian random process (*13*).

We now consider the different ways in which the information signal $s(t)$ can be injected into the transmitter. Note that, unlike the case for the Pecora and Carroll method (*2*), where the information is mixed outside the transmitter, in the systems of concern here $s(t)$ is coupled into the feedback loop of the chaotic oscillator.

There are five possible points of injection, indicated in Fig. 1 by the Roman numerals I, II, III, IV, and V. The addition of $s(t)$ to the feedback loop signal at a given transmitter input point modifies Eq. (2) in accord with the following:

I: $$v(t)+\tau\frac{dv(t)}{dt}=\beta\cdot NL\{f[v(t-T)+s(t)]\} \tag{3}$$

II: $$v(t)+\tau\frac{dv(t)}{dt}=\beta\cdot NL\{f[v(t-T)+s(t-T)]\} \tag{4}$$

III: $$v(t)+\tau\frac{dv(t)}{dt}=\beta\cdot NL\{f[v(t-T)]\}+s(t) \tag{5}$$

IV: $$v(t)+\tau\frac{dv(t)}{dt}=\beta\cdot NL\{f[v(t-T)]\}+\beta\cdot s(t) \tag{6}$$

V: $$v(t)+\tau\frac{dv(t)}{dt}=\beta\cdot NL\{f[v(t-T)]+s(t)\}. \tag{7}$$

It can be seen from Eqs. (3–7) that, in each case, the information signal $s(t)$ changes the dynamics of the entire transmitter and therefore participates in chaos generation. The parameters of the chaotic signal created inside the transmitter thus depend on the parameters of $s(t)$: independent of the choice of the injection point of $s(t)$ in the transmitter and of the point where a part of the chaotic signal is extracted from the transmitter as output, the output signal represents more than simply the superposition of a chaotic signal and the information signal.

There are also five points in the feedback loop where the transmitter output can be obtained. These are indicated in Fig. 1 by Arabic numerals 1 through 5.

The receiver consists of elements identical to those in the transmitter, and with the same topological layout, except that there is no feedback loop: the loop is broken at the receiver input point, i.e., at the point where the signal from the transmitter is inserted. It is critical that the input to the receiver—the encrypted chaotic signal from the transmitter—pass through elements that are effectively identical to those in the transmitter and that are encountered in the same order. Thus, the element in the receiver first encountered by the receiver input must be the same as the element in the transmitter that immediately follows the transmitter output point. Recovery of the original information signal $s(t)$ is achieved by subtracting the signal generated at the output of the receiver from the input encrypted signal. Figure 2 illustrates the transmitter-receiver combination for case II/1. In what follows, we consider this specific case for illustrating the synchronization and decoding process.

Equations (3) through (7) assume that $s(t)$ is directly added to the chaotic signal propagating in the feedback loop. In principle, some other linear or nonlinear combination of $s(t)$ and the chaotic signal in the transmitter can be used, so long as operation performed is invertible. The signal $s(t)$ can then be recovered by using the mathematical operation reciprocal to that used for coupling $s(t)$ into the transmitter. As an example, if a multiplication is used in the transmitter, a division should be made in the receiver. This possibility has recently been treated mathematically by Abarbanel and Kennel in connection with coupled ring lasers (*14*), and verified experimentally by Van Wiggeren and Roy with coupled EDFAs (*8*). Additive or subtractive operations appear to be preferable at radio frequencies, where fast, simple circuitry is desired.

The input to the receiver shown in Fig. 2 is given by $p(t) = v(t - T) + s(t - T)$. The difference-differential equation describing the chaos created in the receiver can be written in the form

$$v'(t)+\tau\frac{dv'(t)}{dt}=\beta\cdot NL\{f[v(t-T)+s(t-T)]\}, \tag{8}$$

where $v'(t)$ is the chaos produced at the output of the time-delay element. Subtraction of Eq. (8) from Eq. (4) yields

$$v(t)+\tau\frac{dv(t)}{dt}-v'(t)-\tau\frac{dv'(t)}{dt}=0, \tag{9}$$

a result that implies that $v'(t) - v(t) = 0$. We thus conclude that the receiver synchronizes to the chaotic part of the signal $p(t)$ from the transmitter, independent of the message signal $s(t)$. (It must be noted that Eq. (9) is obtained for Case I; it is not necessarily valid for the other cases.)

The time required for chaos synchronization can be estimated by considering small deviations $\delta v'(t)$ of $v'(t)$ from $v(t)$, i.e., $v(t) = v'(t) + \delta v'(t)$. From Eqs. (4) and (8) we have $\delta v'(t) + \tau d[\delta v'(t)]/dt = 0$, yielding

$$\lim_{t\to\infty}[v(t)-v'(t)]=\lim_{t\to\infty}[\exp(-t/\tau)]=0.$$

Synchronization (*15*) is achieved asymptotically with a time constant approximated by τ. In the limit, subtracting the chaos $v'(t)$ at the receiver output from the receiver input signal $p(t)$ yields the difference signal

$$\Delta(t) = p(t) - v'(t-T) = s(t-T). \tag{10}$$

It is seen that the system under consideration gives *rigorously* the original information signal $s(t)$, delayed by T. Recovery of the original message depends neither on the parameters of the chaotic carrier (including the number of Lyapunov exponents) nor on the message signal. The method succeeds even if the amplitude of the message signal $s(t)$, its bandwidth, or both, are larger than those of the chaotic carrier. Of course this possibility has no utility in the framework of secure communications and of encryption systems, for which the amplitude of $s(t)$ is chosen very small compared with that of the chaotic carrier. Nevertheless, it is significant that full chaos synchronization is achieved. In addition, the receiver is self-synchronized with the transmitter, since no additional synchronization channel is required.

The results of all possible cases are presented in Table 1. The rigorous solutions $\Delta(t) = s(t)$ and $\Delta(t) = s(t-T)$, which yield an exact copy of the original message signal for any source (i.e., characterized by any linear or nonlinear f-function) and nonlinear element (e.g., with *NL* having any number of extrema) are obtained only in seven cases: those cases that lie along the table diagonal and cases II/1 and IV/3.

Cases III/1, IV/1, III/2, and IV/2 yield difference signals $\Delta(t)$ ruled by differential equations (see Table 1) whose solutions are of the form $\tau\cdot\Delta(t) = s(t) * \exp(-t/\tau)$, where $*$ denotes a convolution. Those solutions are physically equivalent to filtering $s(t)$ by a low-pass filter with a cut-off frequency $1/(2\pi\tau)$. In these cases, the recovery of the message signal $s(t)$ is possible without degradation only if the frequency bandwidth of $s(t)$ is much smaller than $1/(2\pi\tau)$, i.e., much smaller than the bandwidth of the hyperchaotic carrier. It is also to be noted that, in the absence of the message signal (i.e., for $s(t)$), chaos replication occurs if $\Delta(t) \rightarrow 0$, implying that the time required for chaos replication is of the order of τ.

When the f-function characterizing the source is a linear function of the form

$$f[v(t)] = \alpha v(t) + \omega, \tag{11}$$

where α and ω are constants, we meet in cases I/5 and II/5 the conditions of full synchronization, and recovery of $s(t)$ is also exact. Condition (11) leads to the equation of a low-pass filter in cases III/5 and IV/5. In these two last cases, the condition of full synchronization is not strictly met, but $s(t)$ can be recovered with negligible degradation if its bandwidth is much narrower than that of the chaotic carrier.

The other ten cases do not allow the information to be extracted directly from the transmitted signal. Expressions that govern the signal $\Delta(t)$ at the receiver output are given, as examples, below for cases V/1, I/3 and V/3:

V/1
$$\Delta(t) + \tau\frac{d\Delta(t)}{dt} = \beta\cdot NL\{f[v(t-2T)] + s(t-T)\} - \beta\cdot NL\{f[v(t-2T)]\}, \tag{12}$$

I/3
$$\Delta(t) = \beta\cdot NL\{f[v(t-2T) + s(t)]\} - \beta\cdot NL\{f[v(t-T)]\}, \tag{13}$$

V/3 $$\Delta(t) = \beta \cdot NL\{f[v(t-2T)] + s(t)\} - \beta \cdot NL\{f[v(t-T)]\}. \quad (14)$$

In each case, if there is no message $s(t)$ input to the transmitter ($s(t)$ = 0), the receiver is synchronized to the transmitter. However, despite that synchronization, it is not possible to retrieve the message unless special post-processing is employed. As an example of such post-processing, consider the case I/3. Assume that the source is characterized by Eq. (10) and that the nonlinearity is given by $NL(v) = \sin^2(v)$. Solving Eq. (13) yields the following expression for message signal $s(t)$:

$$s(t) = \frac{1}{\alpha}\left\{\sin^{-1}\sqrt{\frac{\Delta(t)}{\beta} + \sin^2[\alpha \cdot v'(t-T) + \omega]} - \omega - \alpha \cdot v'(t-T)\right\}. \quad (15)$$

Note that both $\Delta(t)$ and $v'(t\text{-}T)$ are required to calculate $s(t)$ using this equation.

Consider now the case when the information signal is mixed with the chaotic signal outside the transmitter, as in the Pecora and Carroll method (*2*). Assume, for example, that the message signal is added externally to the chaotic feedback-loop signal produced at the output of the delay element (output 1 in Fig. 1) and input the resultant sum signal to the open-loop receiver at the usual point, i.e., at the input to the controlled source. Analysis of the dynamics of the transmitter-receiver combination yields a difference signal $\Delta(t)$ at the receiver output governed by

$$\Delta(t) + \tau\frac{d[\Delta(t) - s(t)]}{dt} = \beta \cdot NL\{f[v(t-2T)]\} - \beta \cdot NL\{f[v(t-2T) + s(t)]\}. \quad (16)$$

Recovery of message signal $s(t)$ by means of Eq. (16) is at best not straight-forward, and direct access to $s(t)$ is clearly impossible. Thus, despite similarities, this system differs markedly from that of Pecora and Carroll, which is based on chaos synchronization indeed.

To verify the conclusions presented above we conducted numerical simulations, implementing Eqs. (3-7) for the transmitter along with the corresponding receiver equations appropriate for the different configurations. In all cases, the output of the simulation was the function $\Delta(t)$ representing the system output. The source was assumed to have the linear characteristics given by Eq. (11), and the nonlinear element was modeled by a sine-squared mapping. Parameters were set as follows: α = 2.27 MHz/V, ω = 22 MHz, T = 160μs, and τ = 16 μs, a filter response time corresponding to a low-pass filter with a cut-off frequency of about 10 kHz (*16*). The information signal was a sinusoidal signal whose amplitude could be varied and whose frequency (~ 4 kHz) was inside the bandwidth of the chaos produced by the transmitter. This chaotic signal generated by the transmitter is shown in Fig. 3(a).

The difference signal $\Delta(t)$ obtained at the receiver output was calculated numerically for the full-synchronization cases (I/1, II/2, III/3, IV/4, V/5, II/1, and IV/3) and for the partial synchronization cases (III/1, IV/1, III/2, IV/2, I/5, II/5, III/5, and IV/5). In each case different values were tested for the amplitude of $s(t)$. Figure 3(b) shows a typical result, obtained for case II/1 when the amplitude of $s(t)$ was set at 1% of the amplitude (*rms*-value) of chaotic carrier signal generated in the transmitter. Similar error-free signal extraction resulted with the signal amplitude ranging from 0.01% to 100% of that of the chaotic carrier. These results confirm the theoretically-reached conclusion that the chaotic behavior of the receiver synchronizes with the chaotic part of the output of the transmitter and not with its non-chaotic part. Synchronization is fully independent of the amplitude and bandwidth of the message $s(t)$.

A specific situation where post-processing is required to recover the message from the difference signal $\Delta(t)$ is illustrated through the example given in Fig. 3(c), which shows $\Delta(t)$ in the case I/2. The ratio between the amplitude of the message $s(t)$ and the amplitude of the chaotic signal in the transmitter is 10^{-1}. It is seen that chaos synchronization is not obtained, and therefore that direct recovery of $s(t)$ is impossible. We have investigated a wide range of values of the message-to-chaos ratio and observed that direct recovery of the message is impossible even when this ratio is as low as 10^{-4}. This result indicates a very high sensitivity of the synchronization process to the presence of any input signal $s(t)$.

The case of mixing the message signal with the chaotic carrier outside the feedback loop is illustrated in Fig. 4. Figure 4(a) shows the receiver output $\Delta(t)$ for a message-to-chaos ratio of 10^{-2}. For Fig. 4(b) the ratio was $5 \cdot 10^{-1}$. The message signal is more easily observed in the high-ratio case. As in the previous cases, the chaotic dynamics of the transmitter and receiver cannot be synchronized.

The results of the numerical simulations agree completely with the analysis of the delayed-differential equations that govern such chaotic systems. The synchronization process in such systems is either fully insensitive or is highly sensitive to external perturbations, depending on the particular system configuration. Returning to the questions raised earlier in the context of communication systems, we thus reach the following conclusion: Full synchronization of the systems under consideration and, hence, direct recovery of the message without post processing require that the signal input and transmitter output be assigned to suitable points in the transmitter. The synchronization process exhibited with the correct configurations is probably one of the most remarkable features of time-delayed feedback chaotic systems, which can produce high-dimensional chaos with very simple devices. In real transmission systems, the properties of the transmission channel must be considered, as well as a possible mismatch of the transmitter and receiver parameters. Preliminary results, to be reported in a longer article, show that good replication of the recovered message requires a very strict matching of the values of the time delay T in the transmitter and in the receiver.

Figure legends

Fig. 1. Delayed-feedback nonlinear system for generation of chaos.

Roman numerals designate points where a message signal can be injected into the system; arabic numerals designate points where the message-modulated chaotic signal can be tapped for transmission to the receiver system.

Fig. 2. Transmitter-receiver combination for case II/1.

Message signal $s(t)$ is input to the transmitter loop. The output of the receiver, $\Delta(t)$, equals $s(t-T)$ if the receiver system is effectively identical to the transmitter.

Fig. 3. Examples of generated signals.

(a) the chaotic signal generated by the transmitter; (b) the difference signal $\Delta(t)$ obtained for case II/1; (c) the difference signal $\Delta(t)$ for the case I/2.

Fig. 4. The message signal mixing with the chaotic carrier outside the feedback loop.

The receiver output $\Delta(t)$ for a message-to-chaos ratio: (a) of 10^{-2}, (b) of $5 \cdot 10^{-1}$.

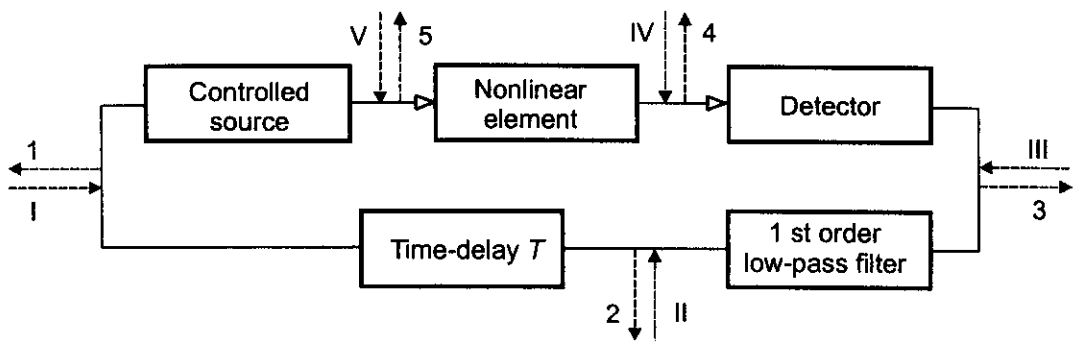
V
5
IV
4
Controlled source
Nonlinear element
Detector
1
I
III
3
Time-delay T
1 st order low-pass filter
2
II

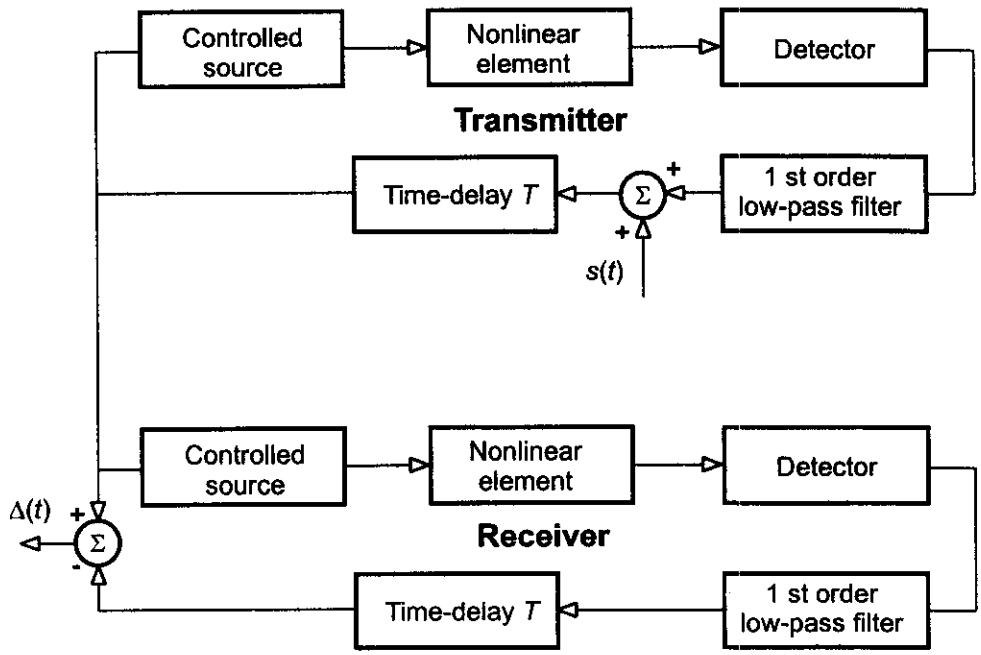
Controlled source
Nonlinear element
Detector
Transmitter
Time-delay T
Σ
+
+
1 st order low-pass filter
s(t)
Controlled source
Nonlinear element
Detector
Δ(t)
+
Σ
-
Receiver
Time-delay T
1 st order low-pass filter

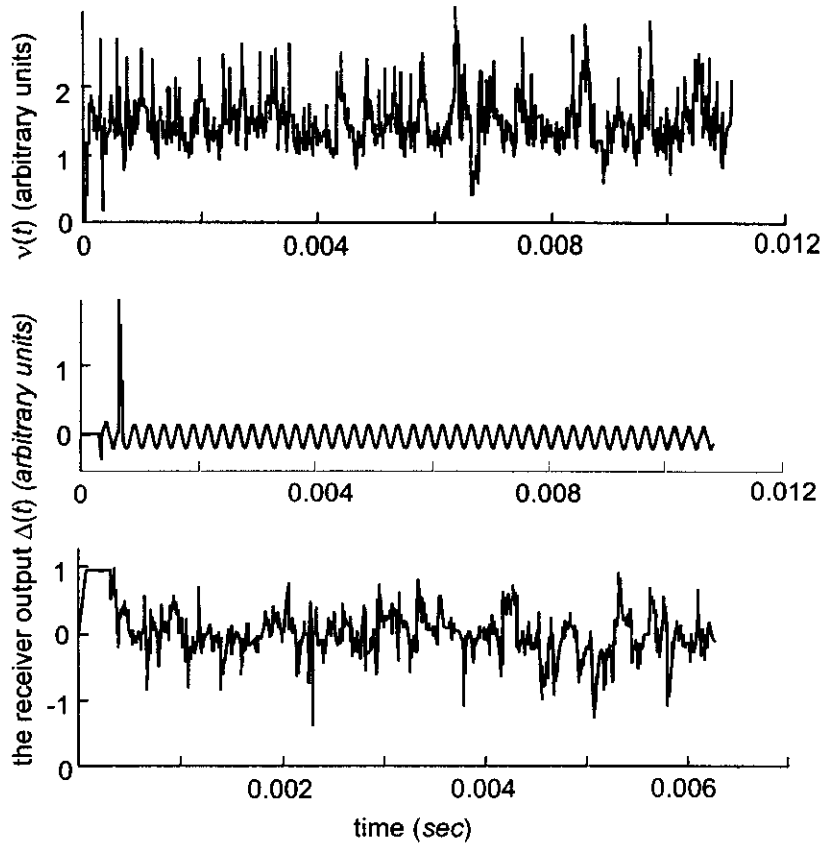
v(t) (arbitrary units)
2
1
0
0
0.004
0.008
0.012
1
0
0
0.004
0.008
0.012
the receiver output Δ(t) (arbitrary units)
1
0
-1
0
0.002
0.004
0.006
time (sec)

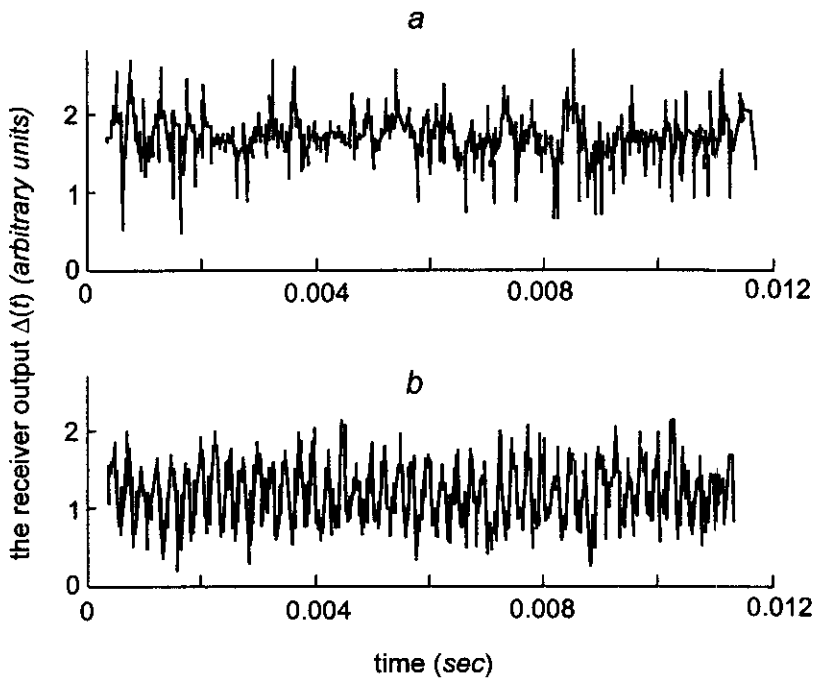
a
b
2
1
0
0
0.004
0.008
0.012
the receiver output Δ(t) (arbitrary units)
time (sec)

J. Phys. III France 3 (1993) 1413-1433

Classification
Physics Abstracts
42.30 — 42.82

Coherence modulation and correlation of stochastic light fields

Jean-Pierre Goedgebuer, Henri Porte and Pascal Mollier

Laboratoire Optique P. M. Duffieux, URA CNRS 214, Faculté des Sciences, Université de Franche-Comté, 25030 Besançon Cedex, France

(*Received 10 December 1992, accepted 5 April 1993*)

Abstract. — We give an overview of the physical principles of coherence modulation of light that are discussed in terms of correlation of stochastic light fields such as those emitted by broadband sources. Multiplexing properties of this method are also considered in the frame of two system topologies, the series and parallel configurations, with emphasis put on source of noise inherent to coherence modulation. Applications are also reviewed in optical telecommunications, optical sensing, integrated optics and optical computing.

1. Introduction.

Coherence modulation of light is a modulation method which utilizes the coherence properties of broadband sources for encoding signals onto a light beam. One peculiarity of the method, compared to other conventional optical modulation methods, is that it allows several signals to be multiplexed on a single light beam. The physical principles make intervene correlation of stochastic light fields that are emitted by broadband sources. This paper is intended as a review of these physical principles, together with a survey of the emerging applications in the area of optical communications, optical computing and integrated optics. We place major emphasis on physical principles of coherence modulation. The paper is organized as follows. In section 2 we show how the well-known phenomenon of « fringes of superposition » can be described in terms of « side lobes of coherence » equivalent to the lateral frequency bands generated by the conventional amplitude and phase modulation techniques in the frequency domain. Section 3 deals with an extension of the previous concepts to the transmission of multiplexed signals. This allows a generalization in section 4 and a discussion on the number of transmission channels and on the dynamic range of coherence-multiplexed systems. In section 5, we show how the coherence modulation process itself induces noise in the detected signals owing to the fact that the mutual degree of coherence of « incoherent » light fields cannot be considered as negligibly small in most cases. Section 6 gives a review of most of the applications of this method which opens new trends in local fiber area network, optical sensing and also in integrated optics in which new devices suitable for coherence modulation begin to appear.

2. Fundamentals of coherence modulation.

2.1 STATISTICAL PROPERTIES OF LIGHT AND COHERENCE DEGREE. — Before specifying the principles of operation of coherence modulation of light, we turn our attention to some well-known statistical properties of the light field emitted by a broadband source, such as a white light source for instance. We assume in the following the power-spectrum of the source is Gaussian, as depicted in figure 1. The center optical frequency is f_0 and full width at half maximum is FWHM = Δf. The notations are given in figures 1a and 1b which show the power-spectrum $P(f - f_0)$ and the coherence degree $|\gamma(t')|$ of a Gaussian white light source. We also recall some properties that will be useful :

1) the light field produced by a continuous white light source is assumed to be a stationary stochastic field with an instantaneous complex amplitude $s(t)$. In the following, the notation used for the covariance function of $s(t)$ is $C(t') = \mathrm{Re}\ \langle s(t) . s^*(t - t')\rangle$, where s^* denotes the complex conjugate of s ;

ii) the coherence degree $|\gamma(t')|$ of the source is defined as the real part of the Fourier Transform of the power-spectrum [1] centered at $f = 0$, normalized to the power P_0 of the source :

$$|\gamma(t')| = \frac{\mathrm{Re} \int_{-\infty}^{+\infty} P(f) \exp(j\, 2\, \pi f t')\, df}{\int_{-\infty}^{+\infty} P(f)\, df} \tag{1}$$

with $\int_{-\infty}^{+\infty} P(f)\, df = P_0$ = power of the source.

After the Wiener-Khintchine theorem, the coherence degree $|\gamma|$ is related to the covariance function $C(t')$ of $s(t)$ by :

$$\mathrm{Re}\ \langle s(t) . s^*(t - t')\rangle = C(t') = P_0 |\gamma(t')| \cos\{2\, \pi f_0 t'\} . \tag{2}$$

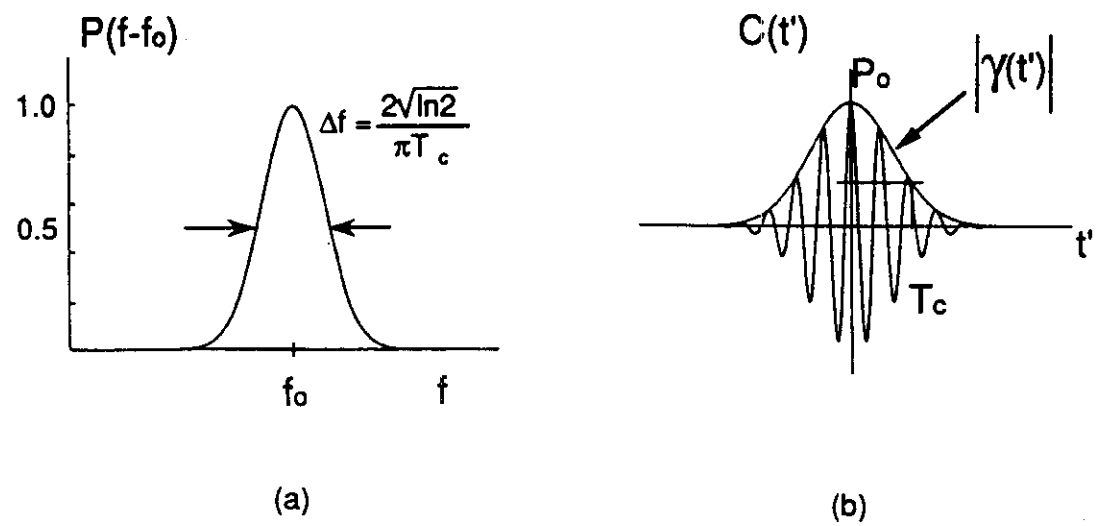

Fig. 1. — (a) Power-spectrum of a Gaussian source. (b) Covariance function of the stochastic light field emitted by the source. The envelope represents the coherence degree $|\gamma|$.

The coherence time T_c of the source is defined in the following as the halfwidth of the coherence degree at e^{-1} of its maximum ; the coherence length is $L_c = cT_c$ (c : velocity of light in vacuum).

For instance, for a source with a Gaussian power-spectrum expressed by :

$$P(f - f_0) = P_0 T_c \sqrt{\pi} \exp \{- \pi^2 T_c^2 (f - f_0)^2\} \tag{3}$$

we have, after equations (1) and (2) :

$$C(t') = P_0 |\gamma(t')| \cos (2 \pi f_0 t') = P_0 \exp \left(- \frac{t'}{T_c} \right)^2 \cos (2 \pi f_0 t') \tag{4}$$

$$|\gamma(t')| = \exp \left(- \frac{t'}{T_c} \right)^2 . \tag{5}$$

2.2 OPTICAL CORRELATION OF STOCHASTIC LIGHT FIELDS. — Equation (2) is important since it shows that the coherence degree $|\gamma|$ can be assessed through the covariance function of the stochastic light fields emitted by a source. We recall briefly how such a covariance function can be obtained experimentally using a Michelson interferometer. In figure 2, a Michelson interferometer with an air-wedge α is illuminated in parallel light by a source whose emitted power is P_0 and power-spectrum is $P(f - f_0)$. The interferometer introduces a variable path-difference D' which corresponds to a time delay $t' = D'/c$ (c : velocity of light). At its output,

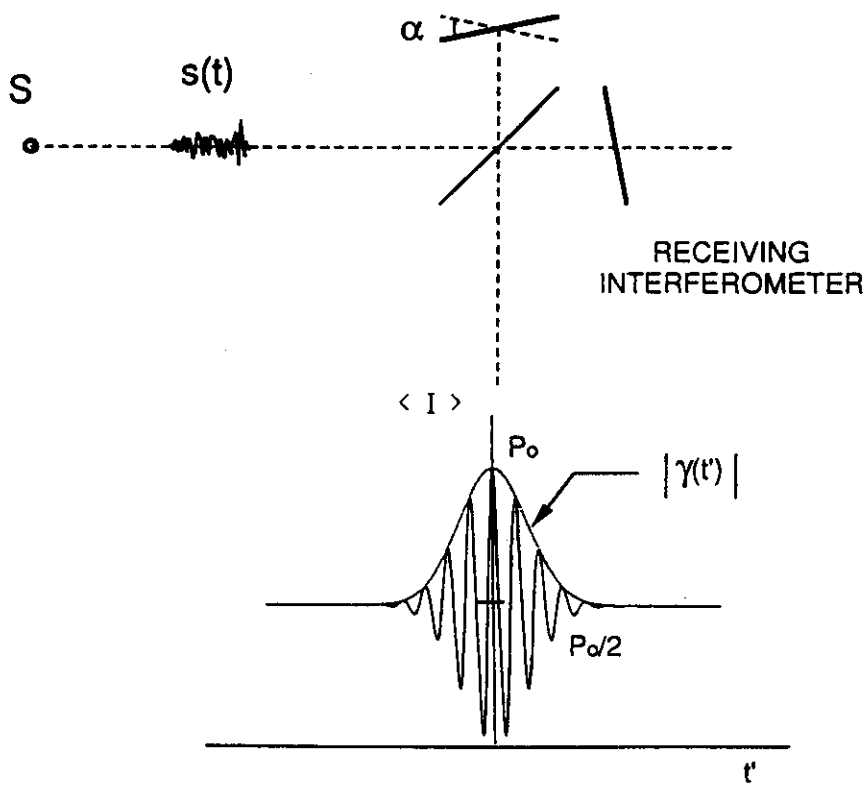

Fig. 2. — Assessing the covariance function of the light field $s(t)$ emitted by source S using a Michelson interferometer. The air-wedge α introduces a variable optical delay t'. The detected energy $\langle I \rangle$ at the output provides the covariance function of $s(t)$.

we obtain two light fields time-delayed by t'. The output light amplitude $f(t)$ is :

$$f(t) = \frac{1}{2} s(t) + \frac{1}{2} s(t - t') . \tag{6}$$

The intensity I detected at the interferometer output results from a time integration performed by the detector :

$$I = \int_0^T |f(t)|^2 \, dt \tag{7}$$

where T is the time integration of the detector. Assuming T is long enough to approximate integral (7) as a time average, the detected intensity is :

$$\langle I \rangle = \langle f(t) . f^*(t) \rangle \tag{8}$$

where $\langle \ \rangle$ denotes a time average.

Substituting equation (6) into (8), we obtain :

$$\langle I(t') \rangle = \frac{1}{4} \langle |s(t)|^2 \rangle + \frac{1}{4} \langle |s(t - t')|^2 \rangle + \frac{1}{4} \langle s(t) . s^*(t - t') \rangle + \frac{1}{4} \langle s^*(t) . s(t - t') \rangle = \frac{1}{2} \langle |s(t)|^2 \rangle + \frac{1}{2} \mathrm{Re} \langle s(t) . s^*(t - t') \rangle \tag{9}$$

where $\langle |s(t)|^2 \rangle = P_0$.

Equation (9) indicates that the intensity $\langle I(t') \rangle$ at the output of the interferometer is the superposition of a dc term $P_0/2$ and the real part of the covariance function of the input light field. The fact that an interferometer can be described in terms of an optical correlator yielding the covariance function of the input light field is a well-known property often used in the area of ultra short light pulses.

However this point is often overlooked in conventional interferometry as continuous wave sources are of concern. For a white light source, the interference pattern observed at the interferometer output is formed by the well-known achromatic Newton's fringes. After equation (2), the latters can be regarded as the physical representation of the covariance function of the stochastic field emitted by the white light source ; the fringe envelope gives the coherence degree $|\gamma(t')|$. In the following, we show how this key property forms the basis the so-called « coherence modulation » of light.

2.3 TOWARDS « COHERENCE MODULATION » OF LIGHT. — The basic principle of coherence modulation of light can be explained from the trivial experiment illustrated in figure 3. In figure 3a, a Mach-Zehnder interferometer is set in front of the Michelson interferometer considered in figure 2. The first interferometer is illuminated in parallel light by the cw white light source S and is adjusted on a path-difference D_1 introducing an optical delay $\tau_1 = D_1/c$ greater than the coherence time of the source. In the following, the Mach-Zehnder interferometer will be termed « coherence modulator », and the Michelson interferometer will be named « receiving interferometer ».

When propagating in the « coherence modulator » as defined above, the light field $s(t)$ emitted by the source is split into twin time-delayed light fields. The light amplitude at the output of the first interferometer is :

$$g(t) = \frac{1}{2} s(t) + \frac{1}{2} s(t - \tau_1) . \tag{10}$$

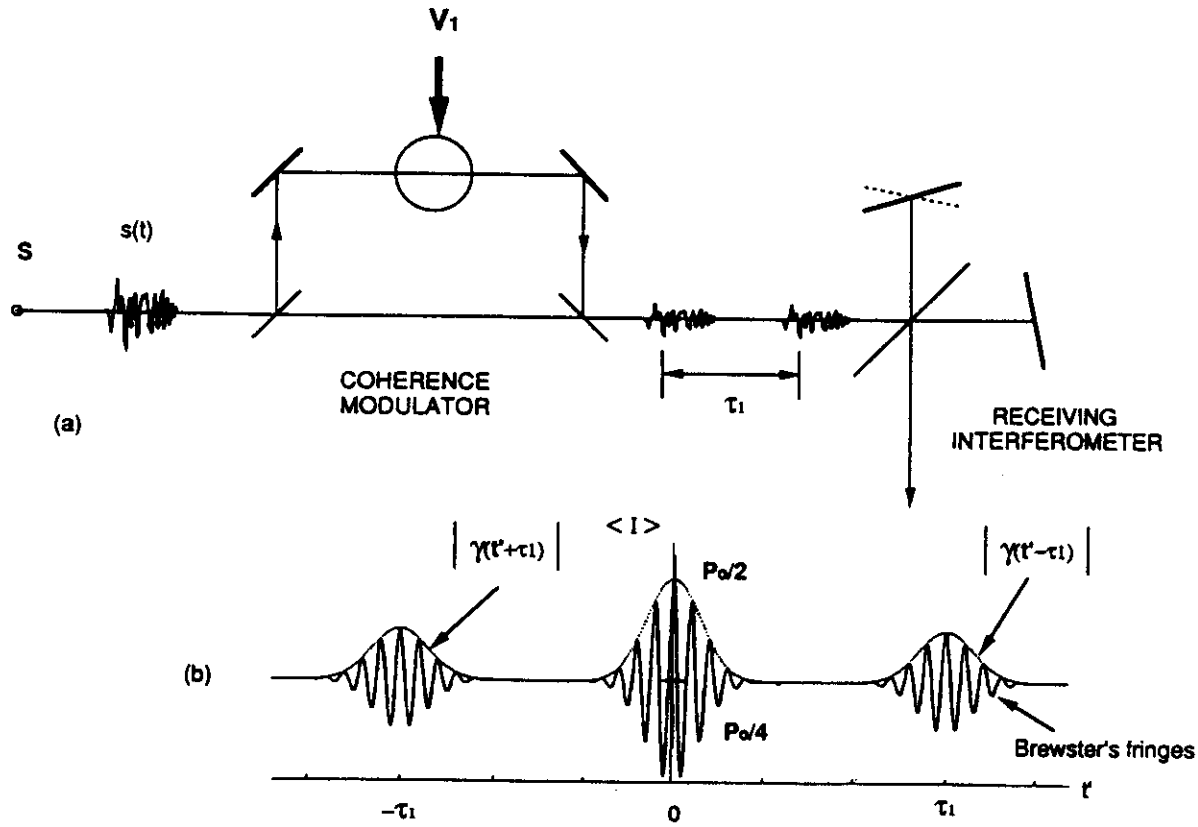

Fig. 3. — (a) Generation of Brewster's fringes using a Mach-Zehnder interferometer in tandem with a Michelson interferometer. (b) Detected power obtained at the output of the Michelson interferometer.

Note here that, in an ideal coherence modulator, no detectable interference fringe is expected since the optical delay τ_1 is greater than the coherence time. In reality a slight intensity modulation subsists due to the low mutual coherence of the twin light fields. The light field $g(t)$ serves as the input of the receiving interferometer.

At the output of the receiving interferometer, which works as an optical correlator as discussed in section 2.2, we obtain the covariance function of the light field $g(t)$. The intensity obtained at the output is given by substituting $s(t)$ by $g(t)$ in equation (9) :

$$\begin{aligned}\langle I(t')\rangle &= \frac{1}{2}\langle|g(t)|^2\rangle + \frac{1}{2}\mathrm{Re}\,\langle g(t).g^*(t-t')\rangle \\ &= \frac{1}{4}\langle|s(t)|^2\rangle + \frac{1}{4}\mathrm{Re}\,\langle s(t)s^*(t-\tau_1)\rangle + \frac{1}{4}\mathrm{Re}\,\langle s(t)s^*(t-t')\rangle + \\ &+ \frac{1}{8}\mathrm{Re}\,\langle s(t).s^*(t+\tau_1-t')\rangle + \frac{1}{8}\mathrm{Re}\,\langle s(t).s^*(t-\tau_1-t')\rangle . \qquad (11)\end{aligned}$$

Using equation (2), this output energy can be expressed as :

$$\langle I(t')\rangle = \frac{1}{4}P_0 + \frac{1}{4}C(\tau_1) + \frac{1}{4}C(t') + \frac{1}{8}C(t'-\tau_1) + \frac{1}{8}C(t'+\tau_1) . \qquad (12)$$

The interference pattern observed at the output of the « receiving interferometer » is the superposition of a uniform background $P_0/4 + C(\tau_1)/4$ and three fringe patterns, as illustrated

in figure 3b located at $t' = 0$ and $t' = \pm \tau_1$. Each fringe pattern represents the covariance function of the white light source.

The side fringe patterns located at $t' = \pm \tau_1$ are the so-called Brewster's fringes or « fringes of superposition » [2]. Their location along t'-axis is directly related to the optical delay τ_1 of the coherence modulator. Such fringes are used for instance in white light interferometry to measure absolute distances or thicknesses of transparent samples [3]. First attempts to use such white light fringes to transmit signals have been reported by C. Delisle and P. Cielo [4].

Why « coherence modulation » of light ?

Whereas such fringes of superposition have been known for a long time, a rather new point of view consists in describing such fringes in terms of coherence modulation of light. Keeping in mind that the intensity obtained at the output of the receiving interferometer is directly related to the coherence degree of its input light, it can be seen from figures 2 and 3 that the « coherence modulator » generates two side lobes of coherence in the light issued from it (these side lobes of coherence are sketched as the envelopes of the Brewster's fringes in Fig. 3). The process may be regarded as being similar to what occurs in conventional amplitude and frequency modulations in which lateral bands are also generated, but in the temporal frequency domain. Detection of the fringes of superposition (= coherence lobes) implies the optical delays τ_1 and t' in the interferometer pair to be matched to within a fraction of the coherence time T_c of the source ; then we have $t' \approx \tau_1$ and the detected energy expressed by equation (12) becomes

$$\langle I(t') \rangle = \frac{1}{4} P_0 \left[1 + \frac{1}{8} \cos 2\pi f_0 (t' - \tau_1) \right] . \tag{13}$$

Assume now the « coherence modulator » in figure 3 has a phase modulator driven by a voltage V_1 in one arm. Then the optical delay τ_1 can vary proportionally to V_1. It can be clearly seen the two side patterns of fringes of superposition (and hence the two side lobes of coherence) will move along t'-axis according to the variations of τ_1. At the output of the receiving interferometer, this results in a detectable intensity modulation which is related to the variations of τ_1, and hence of V_1. Assessing V_1 is achieved by determining the locations of the side lobes of coherence, i.e. of the fringes of superposition at the output of the receiving interferometer. Another possibility is to operate with a photodiode set at the inflexion point of the cos-curve (13) in order to obtain a detected energy directly proportional to V_1. This is achieved with the interferometer pair held in quadrature in order to have a path-mismatch of $\lambda_0/4$: $t' = \tau_1 + 1/4 f_0$. When applying voltage V_1, the optical delay of the « coherence modulator » becomes $\tau_1 + KV_1$ (K is the phase tuning rate of the phase modulator). Then the detected energy takes the form :

$$\langle I(t') \rangle = \frac{1}{4} P_0 [1 + \pi f_0 K V_1] . \tag{14}$$

This expression has been derived assuming $|\gamma(t' - \tau_1)| \approx 1$. It holds if the optical delay induced by the phase modulator is kept smaller than $\lambda_0/4$, i.e., if $V_1 < 1/4Kf_0$. In these circumstances, the system operates in the linear range of the cos-curve which corresponds to the fringes of superposition and the output energy is directly related to the signal V_1. We will explain later how this can be achieved practically for high frequency signals used in optical communications. However the point of view discussed in this section on the basic principles of « coherence modulation » may raise several objections that will be discussed at the end of the article.

Considerations on the advantages provided by « coherence modulation » are given in next section.

3. Coherence multiplexing.

One of the main features of coherence modulation is that it allows optical signal multiplexing to be carried out — that is increasingly important in fiber telecommunication networks.

3.1 PARALLEL COHERENCE MULTIPLEXING. — Figure 4a illustrates the basic principles of a coherence modulated transmission system designed to transmit two signals simultaneously on a single transmission link such as an optical fiber for instance. The system is formed by two « coherence modulators » and the receiving interferometer (optical delay τ') described in section 2.3. Each « coherence modulator » features an optical delay τ_1 and τ_2 greater than the coherence time and is powered by a white light source $S_{1,2}$ which emits a stochastic light field $s_{1,2}(t)$. For clarity, illustration of the situation will be given taking $\tau_2 = 2\,\tau_1$. First, suppose the source S_1 operates. The light field produced by the coherence modulator # 1 is

$$g_1(t) = \frac{1}{2} s_1(t) + \frac{1}{2} s_1(t - \tau_1) .$$

The energy $\langle I \rangle$ at the output of the receiving interferometer is given by replacing s by s_1 in equation (11). Figure 3b shows the interference pattern thus obtained. It exhibits two side lobes of coherence which correspond to the fringes of superposition located at

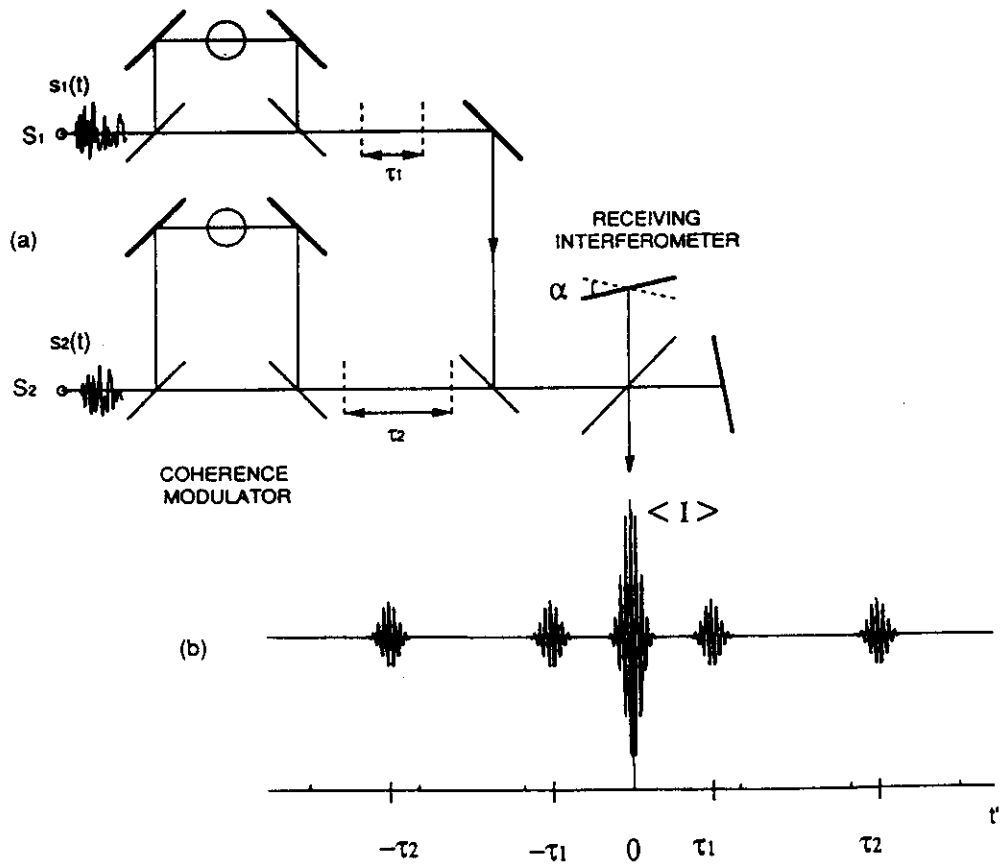

Fig. 4. — (a) Parallel topology for a coherence-multiplexed system. (b) Detected power obtained at the output of the receiving interferometers. The satellite fringes are Brewster's fringes whose localization is related to the optical delays τ_1 and τ_2 of the coherence modulators.

$t' = \pm \tau_1$. Suppose now that the source S_2 only operates. Then the light field obtained at the output of the coherence modulator # 2 is :

$$g_2(t) = \frac{1}{2} s_2(t) + \frac{1}{2} s_2(t - \tau_1) .$$

The two side lobes of coherence are centered at $t' = \pm \tau_2$. Suppose now the two sources S_1 and S_2 operate in parallel. The sources being mutually incoherent, the light fields s_1 and s_2 are not correlated and we have in an ideal system $\langle s_1(t) . s_2^*(t - t') \rangle = 0$. Then the power $\langle I(t') \rangle$ at the output of the reveiving interferometer can be easily deduced from equation (11) :

$$\langle I(t') \rangle = \frac{1}{4} \langle |g_1(t)|^2 \rangle + \frac{1}{4} \langle |g_2(t)|^2 \rangle + \frac{1}{4} \mathrm{Re} \langle g_1(t)\, g_1^*(t - t') \rangle +$$

$$+ \frac{1}{4} \mathrm{Re} \langle g_2(t) . g_2^*(t - t') \rangle = \frac{1}{8} \{P_1 + P_2 + C_1(\tau_1) + C_2(\tau_2)\}$$

$$+ \frac{1}{8} C_1(t') + \frac{1}{8} C_2(t') + \frac{1}{16} C_1(t' \pm \tau_1) + \frac{1}{16} C_2(t' \pm \tau_2) \qquad (15)$$

with P_1, P_2 power of the sources 1 and 2.

The interference pattern thus obtained is formed by the incoherent superposition of the previous interference patterns as shown in figure 4b. We obtain now four side lobes of coherence centered at $t' = \pm \tau_1$ and $t' = \pm \tau_2$ respectively. Then, transmission and detection of two electric signals V_1 and V_2 is carried out by determining the locations of the fringes of superposition obtained at the receiving interferometer. This can be extended to a number of N signals by using an array of N parallel coherence modulators powered by N sources. This multiplexing scheme offers the greatest potential in optical telecommunications and sensor arrays with the possibility of using sources with no stringent requirements on the source linewidth and on the center frequency of laser emission, in contrast to wavelength multiplexing and demultiplexing methods.

3.2 SERIES COHERENCE MULTIPLEXING. — Figure 5a shows another coherence multiplexing scheme in which the « coherence modulators » are now set in cascade. For simplicity, we limit the discussion to only two « coherence modulators » but it can be extended to a cascade with a higher number of modulators. Each coherence modulator features an optical delay τ_1 and τ_2 greater than the coherence time. For clarity, the situation is illustrated taking $\tau_2 = 3\ \tau_1$. The situation is completely different from the previous case in so far as the light emitted by the first coherence modulator is used as the input of the second one. Then, the light fields can be written as :

* output of coherence modulator # 1 :

$$g_1(t) = \frac{1}{2} s(t) + \frac{1}{2} s(t - \tau_1) \qquad (16)$$

* output of coherence modulator # 2 :

$$g_2(t) = \frac{1}{2} g_1(t) + \frac{1}{2} g_1(t - \tau_2) . \qquad (17)$$

This light field serves as the input of the receiving interferometer.

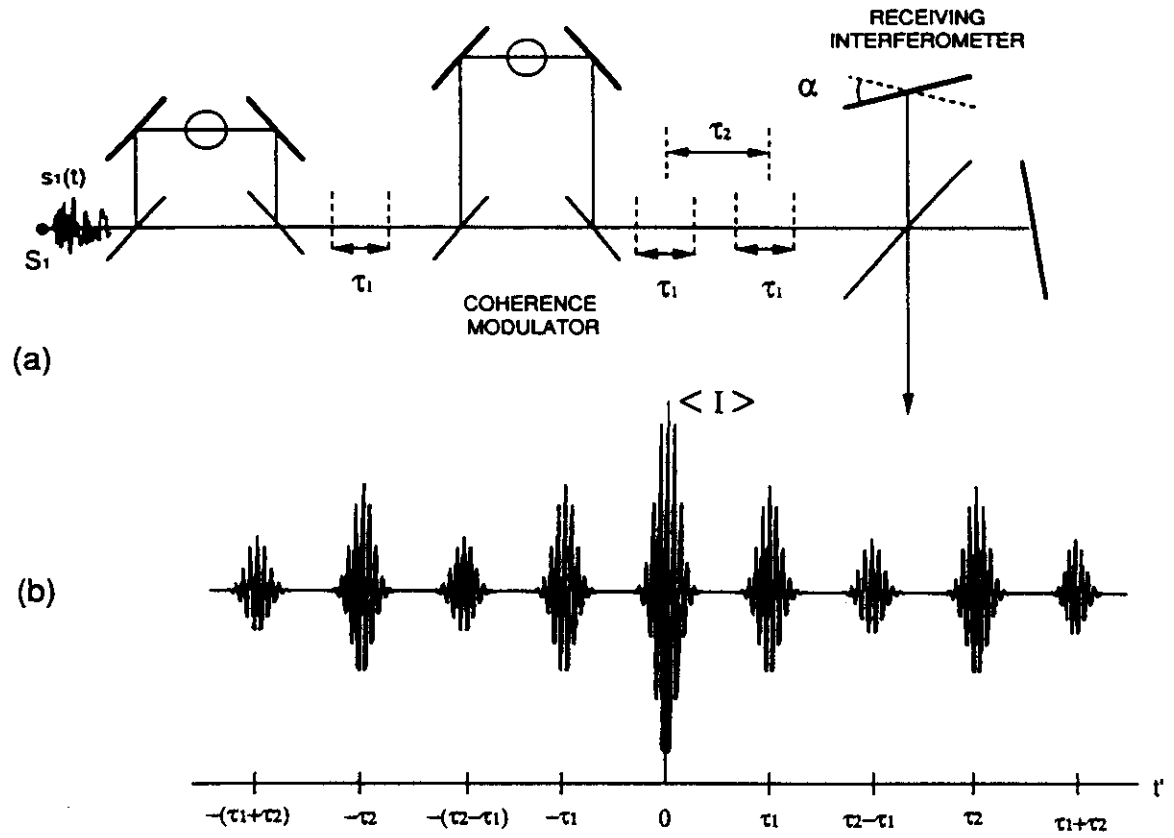

Fig. 5. — (a) Series topology for a coherence-multiplexed system. (b) Detected power at the output of the receiving interferometer. Signal Brewster's fringes ($\pm \tau_1$, $\pm \tau_2$) are obtained together with cross-term Brewster's fringes ($\pm \tau_1 \pm \tau_2$).

Thus, after equation (11), the power $\langle I(t') \rangle$ at the output of the receiving interferometer is related to the covariance function of $g_2(t)$ by :

$$\langle I(t') \rangle = \frac{1}{2} \left\langle |g_2(t)|^2 \right\rangle + \frac{1}{2} \operatorname{Re} \langle g_2(t) \, . \, g_2^*(t - t') \rangle \, . \tag{18}$$

Finally, we obtain :

$$\begin{aligned} \langle I(t') \rangle = & \left[\frac{1}{8} P_0 + \frac{1}{8} C(\tau_1) + \frac{1}{8} C(\tau_2) + \frac{1}{16} C(\tau_1 + \tau_2) + \frac{1}{16} C(\tau_2 - \tau_1) \right] + \\ & + \left[\frac{1}{8} C(t') + \frac{1}{16} C(t' \pm \tau_1) + \frac{1}{16} C(t' \pm \tau_2) \right. \\ & \left. + \frac{1}{32} C\{t' \pm (\tau_2 - \tau_1)\} + \frac{1}{32} C\{t' \pm (\tau_1 + \tau_2)\} \right] . \end{aligned} \tag{19}$$

Figure 5b shows the interference pattern thus obtained. The terms in the first brackets represent a dc term. The covariance function C decaying with optical delay, the value of the dc term can be approximated to $P_0/8$. The terms in the second brackets represent nine packets of fringes of superposition located at $t' = 0$, $\pm \tau_1$, $\pm \tau_2$, $\pm (\tau_2 - \tau_1)$ and $\pm (\tau_1 + \tau_2)$. Obviously, signal demultiplexing is carried out using the fringes located at $t' = \pm \tau_1$ and $t' = \pm \tau_2$. The other fringes which are located at $\pm \tau_2 \pm \tau_1$ correspond to cross-terms which may cause crosstalk as will be discussed in paragraph 5.2.

The situation becomes very complex when increasing the number of coherence modulators. The values of the optical delays $\tau_1, \tau_2, \ldots, \tau_N$ must be chosen very carefully, as will be discussed in section 5.3. At the output of the receiving interferometer, the interference pattern thus obtained is formed by packets of fringes located at $t' = \tau_1, \tau_2, \ldots, \tau_N$ and also at all combinations such as $t' = \pm \tau_i \pm \tau_j$, $t' = \pm \tau_i \pm \tau_j \pm \tau_k$, etc... The fringes of interest for signal demultiplexing are those located at $t' = \tau_1, \tau_2, \ldots, \tau_N$. A practical implementation of such an array of coherence modulators will be illustrated in the area of optical communications in section 6.

4. Generalization to N coherence-multiplexed signals.

In previous sections, the discussion was limited to systems with only two channels for simplicity's sake in order to point out the physical background. However in an effective transmission system, one may wonder what is the evolution of the detected signals, especially in terms of dynamic range and modulation depth, as the number of channels increases.

4.1 PARALLEL CONFIGURATIONS WITH N CHANNELS. — Consider N « coherence modulators » with optical delays $\tau_1, \tau_2, \ldots, \tau_N$, powered in parallel by N sources. We assume that light produced by such modulators is launched in a receiving interferometer *via* a $N \times 1$ coupler (N inputs, 1 output). The optical delay of the receiving interferometer is t'. The light field at the output of the i-th modulator is, after equation (13) :

$$g_i(t) = \frac{1}{2} s_i(t) + \frac{1}{2} s_i(t - \tau_i) \tag{20}$$

where $s_i(t)$ is the light field emitted by source S_i. The resulting light field $g(t)$ at the entrance of the receiving interferometer is :

$$g(t) = \frac{1}{\sqrt{N}} \cdot \sum_{i=1}^{N} g_i(t) . \tag{21}$$

The term $1/\sqrt{N}$ appears because of the unavoidable losses which occur when light fields from N sources are combined by a $N \times 1$ coupler. Then, for an ideal system powered by mutually incoherent sources, the power detected at the output of the receiving interferometer is, after equation (15) :

$$\begin{aligned} \langle I(t') \rangle &= \frac{1}{2} |g(t)|^2 + \frac{1}{2} \operatorname{Re} \langle g(t)\, g^*(t - t') \rangle \\ &= \frac{1}{4N} \left[\sum_{i=1}^{N} \left\{ P_i + C_i(\tau_i) + C_i(t') + \frac{1}{2} C_i(t' \pm \tau_i) \right\} \right] . \end{aligned} \tag{22}$$

The two first terms correspond to a dc term whose value can be approximated to $\Sigma P_i/4N$. The last terms correspond to $2N$ patterns of fringes of superposition centered at $t' = \pm \tau_1, \pm \tau_2, \ldots, \pm \tau_N$. The fringe frequency in each pattern is related to the center frequency of the corresponding source. As an illustration, the interference pattern thus obtained is sketched in figure 6 for $N = 4$ channels which have optical delays ruled by the arithmetic series 1, 2, 3, 4. As the receiving interferometer is closely matched to the i-th channel ($t' \approx \tau_i$), and assuming the sources have the same power P_0, the detected power takes the form :

$$\langle I(t') \rangle = \frac{P_0}{4} \left[1 + \frac{1}{2N} \cos \left\{ 2\pi f_0 (t' - \tau_i) \right\} \right] . \tag{23}$$

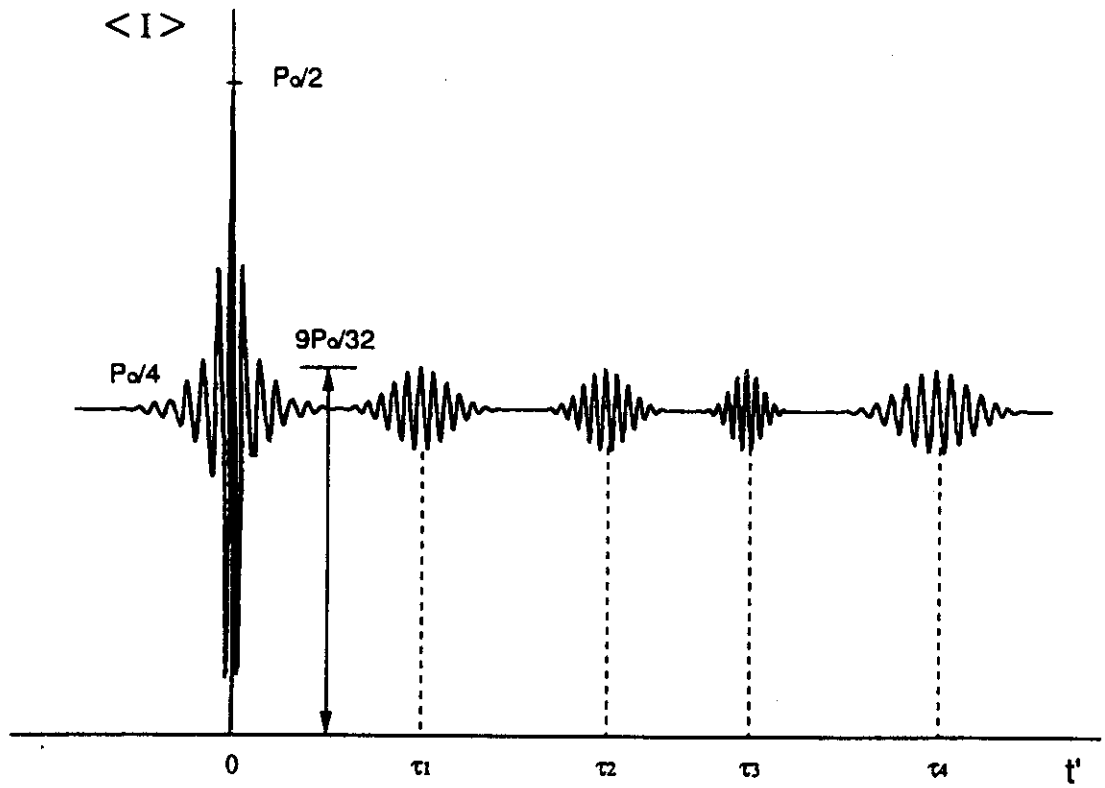

Fig. 6. — Detected power obtained at the output of the receiving interferometer *vs.* its optical delay, for a four-channel parallel system designed with carriers τ_1, $2\,\tau_1$, $3\,\tau_1$, $4\,\tau_1$.

This expression has been derived by setting $|\gamma'(t' - \tau_i)| = 1$ and $C_i(\tau_i)$, $C_i(t')$, $C_i(t' + \tau_i) = 0$ for an ideal system with no crosstalk (this latter point is justified in Sect. 5). Expression (23) shows that the modulation depth is $1/2\,N$ and, hence, decreases with increasing the number of channels. This poses a limit to the maximum number of channels in parallel topologies.

4.2 SERIES CONFIGURATIONS WITH N CHANNELS. — Consider an array of coherence-multiplexed emitters formed by N cascaded « coherence modulators » with optical delays $\tau_1, \tau_2, \ldots, \tau_N$, in tandem with a receiving interferometer with an optical delay t'. The system is powered by a single source with power P_0. The light at the output of the series of the N modulators can be expressed *via* a series of convolution products :

$$g(t) = s(t) \otimes \frac{1}{2}\left\{\delta(t) + \delta(t - \tau_1)\right\} \otimes \frac{1}{2}\left\{\delta(t) + \delta(t - \tau_2)\right\} \otimes$$
$$\otimes \cdots \otimes \frac{1}{2}\left\{\delta(t) + \delta(t - \tau_N)\right\} = \frac{1}{2^N} s(t) \otimes \prod_{i=1}^{N} \left\{\delta(t) + \delta(t - \tau_i)\right\} \qquad (24)$$

where $s(t)$ is the initial light field emitted by the source, $\otimes$ stands for a convolution products and $\prod$ for a series of convolution products. The light field $g(t)$ serves as the input of the

receiving interferometer. Then the power detected at its output is, after equation (18) :

$$\langle I(t')\rangle = \frac{1}{2}|g(t)|^2 + \frac{1}{2}\,\mathrm{Re}\,\langle g(t)\,g^*(t-t')\rangle$$

$$= \frac{1}{2^{2N+1}}\left[2^N P_0 + \mathrm{Re}\,\langle s(t)\,s^*(t-t')\rangle \otimes \prod_{i=1}^{N}\{2\,\delta(t') + \delta(t' \pm \tau_i)\}\right]. \quad (25)$$

The interference pattern described by expression (25) is formed by a uniform background $P_0/2^{N+1}$ with patterns of fringes of superposition corresponding to the second term. A full analysis of this latter term [5] shows that it corresponds to 3^N groups of fringes of superposition located at $t' = 0, \pm\tau_1, \pm\tau_2, \ldots, \pm\tau_N$ and at all combinations such as $t' = \pm(\tau_i \pm \tau_j \pm \tau_k)$, $t' = \pm(\tau_i \pm \tau_j \pm \cdots \pm \tau_N)$, etc. The signal fringes used for the demultiplexing process are those located at $t' = \pm\tau_1, \ldots, \pm\tau_N$ while the others are cross-term fringes. Sakai and Parry [6] have proposed a more compact form to express the optical delays corresponding to these cross-term fringes :

$$t' = \sum_{i=1}^{N} \varepsilon_i\,\tau_i \quad (26)$$

where $\varepsilon_i \in \{-1, 0, 1\}$ and $\sum_{i=1}^{N} \varepsilon_i^2 \neq 1$.

The optical delays τ_i in the modulators must be chosen such that none of them is a member of the set defined in (26). This point is discussed in paragraph 5.3. As an illustration, figure 7 shows the interference pattern obtained for a three channel system with optical delays τ_1, $\tau_2 = 3\,\tau_1$ and $\tau_3 = 8\,\tau_1$.

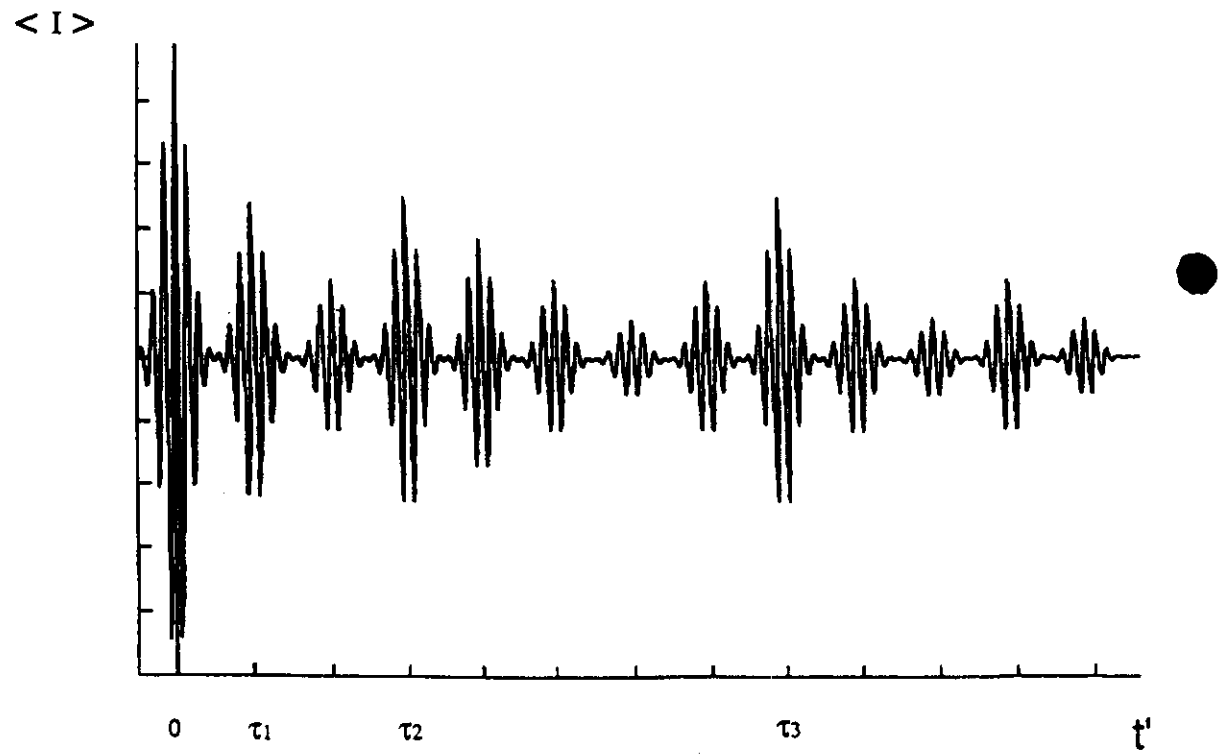

Fig. 7. — Detected power obtained at the output of the receiving interferometer *vs.* its optical delay, for a three-channel series system designed with carriers τ_1, $3\,\tau_1$, $8\,\tau_1$.

Assume now the receiving interferometer is closely matched to the i-th coherence modulator : $t' \approx \tau_i$. Then the detected power reduces to :

$$\langle I(t') \rangle = \frac{P_0}{2^{N+1}} \left[1 + \frac{1}{2} \cos \{ 2 \pi f_0 (t' - \tau_i) \} \right] . \quad (27)$$

Expression (27) is the response of the receiving interferometer for an ideal system with no crosstalk. It shows that the modulation depth is 50 % and, hence, is independent of the number N of channels whereas the modulation depth decreases proportionaly to $1/2\,N$ with increasing N in the parallel topology. The series scheme is more advantageous from that point of view. However note that the signal power is $1/2^{N+2}$ and, hence, decreases more rapidly with increasing the number of channels than in the parallel configuration in which the signal power is $1/8\,N$. Practically it means that a series configuration requires photodetectors with very low sensitivity while a parallel configuration requires photodetectors exhibiting a wide dynamic range.

5. Noise in coherence-modulated systems.

In this section, we limit the discussion to noise generated by the physical process attached to coherence modulation itself. We do not consider electrical or phase noise associated to photodetectors or environmental conditions.

5.1 PHASE-INDUCED INTENSITY NOISE. — When interferometers with gross path mismatch greater than the coherence length are used, the « incoherent » light fields which mix from the various optical paths still interfere due to their mutual coherence which cannot be considered as negligibly small. It results in an intensity noise which is generated physically by the random fluctuations of the phase of the initial light field emitted by the source. This noise is termed « phase-induced intensity noise ». It can be ascertained by returning to the single coherence-modulated interferometer pair shown in figure 3 and by assuming the two interferometers have their optical delays matched one to each other within a fraction of the coherence time : $t' \approx \tau_1$. Then the detected signal at the system output is given by, after equations (12) and (4) :

$$\langle I(t') \rangle = \frac{P_0}{8} \{ 2 + |\gamma(t' - \tau_1)| \cos [2 \pi f_0 (t' - \tau_1)] + 2 |\gamma(\tau_1)| \cos [2 \pi f_0 \tau_1] + $$

$$+ 2 |\gamma(t')| \cos [2 \pi f_0 t'] + |\gamma(t' + \tau_1)| \cos [2 \pi f_0 (t' + \tau_1)] \} \quad (28)$$

and finally we have, taking $|\gamma(t' - \tau_1)| = 1$ and neglecting the three last terms :

$$\langle I(t') \rangle = \frac{P_0}{8} \{ 2 + \cos [2 \pi f_0 (t' - \tau_1)] \} . \quad (29)$$

In reality, in taking the mean power $\langle I \rangle$ as the expected value of the detected signal, we have assumed the detector has an infinite time of integration and, hence, we have averaged out the signal intensity noise $I - \langle I \rangle$ which is present in practice. The latter can be ascertained from calculations reported by Kersey and Dandridge [7]. Figure 8 shows the results for a single unbalanced Mach-Zehnder interferometer powered by laser diodes with various coherence lengths. The noise level peaks when the optical path difference equals the coherence length L_c, and decreases beyond L_c.

Coming back to our interferometer pair, it can be clearly seen now why the three last terms in equation (28), which denote the contributions of $|\gamma(\tau_1)|$ and $|\gamma(2\,\tau_1)|$, are principally

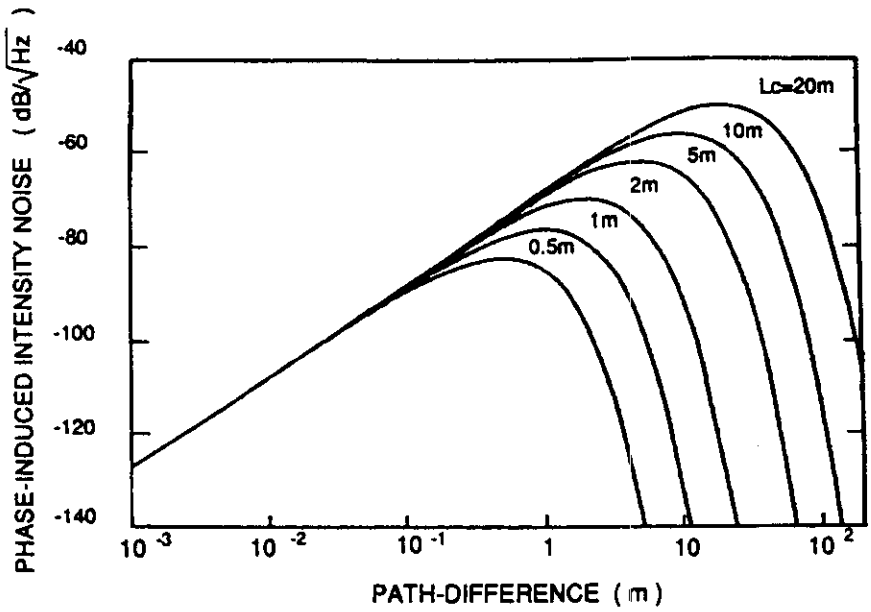

Fig. 8. — Phase-induced intensity noise obtained with an unbalanced Mach-Zehnder interferometer, for different values of the coherence length (after Kersey and Dandridge [7]).

responsible for the generation of this excess noise. Hence, low noise levels imply the use of large optical delays and short coherence lengths.

The statistical nature of this noise depends on the number of interferometers and on the system topology, as well as on the nature of the initial phase noise of the source. The latter can be modeled as a Wiener-Levy stochastic process for a single mode laser diode, or as a Gaussian random process for a thermal source. Considerations on the spectral power density of this noise are reported by Brooks *et al.* [8], and Wentworth [9] for singlemode laser diodes, thermal sources, superluminescent diodes and multimode laser diodes.

5.2 INTERMODULATION NOISE. — This type of noise appears when several signals are coherence-multiplexed. This results in crosstalk between the signals. In parallel configurations, this can be evaluated from figure 4, in which two « coherence modulators » are used in parallel to perform coherence multiplexing. Assume the receiving interferometer is matched to coherence modulator # 2 within a fraction of the coherence time : $t' \approx \tau_2$. Under these conditions, the detected output power is, after equation (15) :

$$\langle I(t')\rangle = \frac{1}{8}P_1 + \frac{1}{8}P_2 + \frac{1}{16}P_2\,|\gamma_2(t' \pm \tau_2)|\cos\,[2\,\pi f_2(t' \pm \tau_2)] +$$

$$+ \frac{1}{16}P_1\,|\gamma_1(\tau_1)|\cos\,[2\,\pi f_1\,\tau_1] + \frac{1}{16}P_1\,|\gamma_1(t' \pm \tau_1)|\cos\,[2\,\pi f_1(t' \pm \tau_1)]$$

$$+ \frac{1}{8}P_1\,|\gamma_1(t')|\cos\,[2\,\pi f_1\,t'] + \frac{1}{8}P_2\,|\gamma_2(t')|\cos\,[2\,\pi f_2\,t']$$

$$+ \frac{1}{16}P_2\,|\gamma_2(\tau_2)|\cos\,[2\,\pi f_2\,\tau_2]\,. \qquad (30)$$

In the ideal case, $|\gamma_{1,2}(\tau_{1,2})|$, $|\gamma_{1,2}(t' + \tau_{1,2})| = 0$ and $|\gamma_2(t' - \tau_2)| = 1$. Then, the output power has the form :

$$\langle I(t')\rangle = \frac{1}{8}P_1 + \frac{1}{8}P_2 + \frac{1}{16}P_2\cos\,\{2\,\pi f_2(t' - \tau_2)\}\,. \qquad (31)$$

This expression represents the idealized response of the receiving interferometer matched to coherence modulator # 2. In reality, however, crosstalk results owing to the interferometric conversion of the phase delay τ_1 produced by coherence modulator # 1. The third term in equation (30), which denotes the contribution from $|\gamma_1(\tau_1)|$ attached to modulator # 1, is responsible for the generation of this crosstalk.

The maximum amplitude of this crosstalk is $|\gamma_1(\tau_1)|$. A second source of crosstalk comes from the fifth term *via* $|\gamma_1(t' - \tau_1)|$. Hence, crosstalk can be decreased to any desired level by using large values of τ_1 and of $t' - \tau_1$ (or of $\tau_2 - \tau_1$ since $t' = \tau_2$ in the example used). Another important conclusion is that crosstalk level is closely related to the profile of the coherence degree of the source, and, hence, to the profile of its spectral line. As an illustration, figure 9 shows the evolution of crosstalk for a parallel coherence-multiplexed system formed by two coherence modulators with optical delays τ_1, $\tau_2 = 2\,\tau_1$, powered by sources exhibiting identical coherence lengths but with Gaussian, Lorentzian and $\cos^2$ spectra. This shows clearly that crosstalk decreases with increasing τ_1, and may vary by several orders of magnitude according to the type of sources used.

The situation is very similar in series systems. Referring to figure 5b, it can be seen that when the receiving interferometer is matched to coherence modulator # 2 ($t' = \tau_2$) for instance, the detected power is corrupted by intermodulation noise generated principally by the satellite lobes of coherence centered at $t' = \tau_1 + \tau_2$ and $t' = \tau_2 - \tau_1$. These satellite lobes of coherence, which feature a Gaussian profile in the model used, are responsible for the generation of crosstalk. Here also, crosstalk is closely related to the values of the optical delays

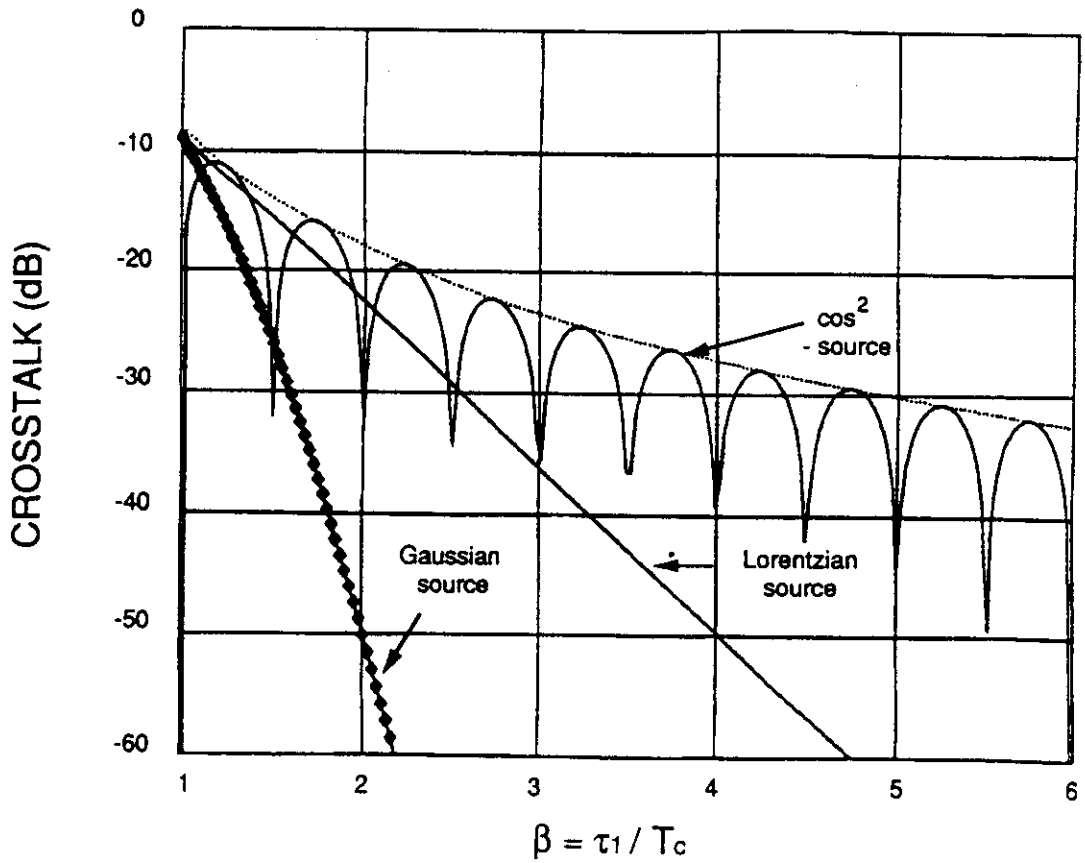

Fig. 9. — Intermodulation noise in a coherence-multiplexed system for different lineshapes.

τ_1, τ_2 set in cascade, and also to the profile of the power-spectrum of the source. A complete discussion can be found in reference [10], in which it is shown that crosstalk down to −30 dB can be easily achieved in practical systems. This opens up straightforward applications in the area of optical communications in which stringent conditions on crosstalk are generally required.

5.3 PERMISSIBLE OPTICAL DELAYS. — The sequence of optical delays is another key point of coherence multiplexing since it determines the phase-induced intensity noise and intermodulation noise. As mentioned above, no overlap should occur between the satellite lobes of coherence in order to prevent channel crosstalk. Hence, the choice of the permissible optical delays introduced in the « coherence modulators » is of major importance. Another issue relevant to the design of a coherence multiplexed system is the compacity of the system, i.e., the maximum possible value of the optical delay.

This maximum value depends on the nature of the interferometers : polarimetric interferometers featuring optical delays greater than some centimeters seem non practicable, while optical delays up to several meters can be implemented using fiber Mach-Zehnder interferometers. Compact sequences of optical delays are required especially for systems with a high number of modulators. The nature of the system determines the sequence of optical delays, as discussed hereafter.

Parallel architectures. — If the crosstalk level has to be identical in each channel, the lobes of coherence corresponding to each of the channels as shown in figure 4 have to be equidistant. Obviously, this means that the sequence of permissible optical delays for a system with N channels must be ruled by the arithmetic series of numbers $m_i = 1, 2, 3, \ldots, N$. If τ_1 is the starting value of the first optical delay, the permissible optical delays are :

$$\tau_1, 2\,\tau_1, 3\,\tau_1, \ldots, N\tau_1 . \tag{32}$$

The starting value τ_1 is determined according to the level of crosstalk tolerable in each of the channels. It can be deduced from figure 9. For instance, for Gaussian sources, a crosstalk of − 25 dB is obtained when the ratio between τ_1 and the coherence time T_c is $\beta = \tau_1/T_c = 1.5$. For a source with a coherence length $L_c = cT_c = 30$ micrometers (e.g. a superluminescent diode), this implies the path-difference $D_1 = c\tau_1$ of the first « coherence modulator » to be 45 micrometers, then the other permissible path-differences expressed in micrometers are 90, 135, 180, 225, ...

Series architectures. — Analysis of the permissible optical delays which lead to a tolerable amount of crosstalk in each channel of series topologies is much more complex than in parallel configurations. The output signal of the receiving interferometer contains a number of spurious intermodulation terms attached principally to the cross-term fringes of superposition defined in paragraph 3.2. The optical delay τ_i of the i-th interferometer in the array must be chosen so that there is no overlap between these cross-term signals and the desired signal from this interferometer. A detailed analysis of the permissible optical delays is given by Blotekjaer *et al.* [11]. It is shown that the suitable optical delays τ_i ($i = 1, 2, \ldots, N$) must be chosen such that none of them is a member of the set of time delays defined in equation (26) which correspond to the cross-term lobes of coherence. This problem of choosing these permissible optical delays does not have a unique solution. The solutions all exhibit exponential growth which severely limits the number of transmitters which may be arrayed in series. We give hereafter two of the possible recursive expressions for possible choices of series of numbers m_i :

$$m_i = \frac{1}{\sqrt{5}}\left[\left(\frac{3+\sqrt{5}}{2}\right)^i - \left(\frac{3-\sqrt{5}}{2}\right)^i\right] \approx 1.17\,.\,(2.618)^{i-1} \tag{33}$$

$$m_i = \begin{cases} 3.2^{N-1} - 2^{N-i} - 2^{1+N/2} + 2 & \text{for } N = 2, 4, 6... \\ 3.2^{N-1} - 2^{N-i} - 3.2^{(N-1)/2} + 2 & \text{for } N = 3, 5, 7... \end{cases} \quad (34)$$

where N is the number of channels.

Series (33) is derived from the recursive expression (26) proposed by Sakai and Parry [6], expressed in closed form by Brooks *et al.* [8]. Series (34) is given by Blotejkaer *et al.* [11]. As an example, we show the two series for a twelve channel system :

Series (33)	1	3	8	21	55	144	377	987	2 584	6 765	17 711	46 368
Series (34)	3 970	4 994	5 506	5 762	5 890	5 954	5 986	6 002	6 010	6 014	6 016	6 018

We observe that series (34) has the smallest m_{12}, i.e., the smallest maximum optical delay. Hence series (34) is more compact and more advantageous in the sense that it allows shorter optical delays. However in series (33), the terms do not depend explicitly on the number of channels and, hence, for a system designed for a given channels, more channels can be added without changing the optical delays of the existing channels. In contrast, if another channel is to be added in a system designed using series (34), the system requires complete redesign. The starting value τ_1 is still determined using the curves of figure 9 which can be extended to series architectures. For instance, for a 12-channel system ruled by series (33) and powered by a Gaussian source with a coherence length $L_c = 30$ micrometers (e.g. a superluminescent diode), crosstalk of -25 dB requires a starting value of $\tau_1 = 45$ micrometers and a maximum optical delay of $\tau_{12} = 270\,765$ micrometers. This shows clearly a practical limitation of the number of transmitters, that is a drawback in comparison with parallel topologies. Note however that series topologies are unique known configurations allowing signals to be multiplexed optically with a single source.

6. Applications.

6.1 INTEGRATED COHERENCE MODULATORS. — The previous sections show that coherence multiplexing can play an important role in the future networks for optical communications. However the construction of modulators matched to coherence modulation is the most serious problem at present. Bulk electro-optic modulators based on Pockels effects in birefringent materials have been proposed to demonstrate the parallel and series topologies and to verify the basic concepts in multimode and single mode fiber transmissions [10, 12, 13]. Integrated phase modulators inserted in one arm of fiber Mach-Zehnder interferometers having a large path-imbalance is a tentative solution usable for demonstration purposes only. The sensitivity of such devices to temperature or to mechanical vibrations is a major drawback. Integrated Mach-Zehnder type modulators could be used. However, their geometry is usually designed to introduce slight imbalanced paths ($< \lambda/4$), yielding optical delays much smaller than the coherence length of the source.

Hence, new integrated modulators have to be developed. An $LiNbO_3$ integrated Mach-Zehnder interferometer with a large path-imbalance between the arms has been proposed recently [14]. The device is shown in figure 10. The path-imbalance is created by a proton exchanged process located on one arm. Proton exchange between Li^+ ions from lithium niobate and H^+ protons from an acid source (e.g. melted benzoic acid in which one arm of the interferometer is immersed) occurs to yield a new propagation medium ($H_xLi_{1-x}NbO_3$) with an extraordinary refractive index higher than that of lithium niobate. Hence, the proton exchange process modifies the effective index of the guided mode. Path-differences of several

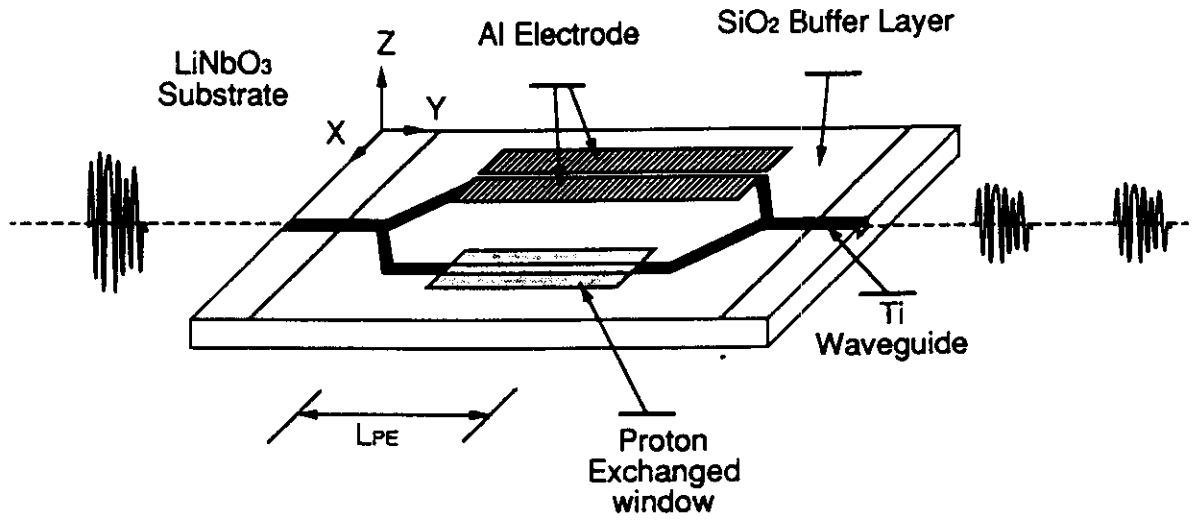

Fig. 10. — Coherence modulator integrated on a $LiNbO_3$ substrate.

hundreds of micrometers can be obtained. The electrodes on the other arm induce an electric field which, in turn, results in a modulation of the effective index of the guided wave by Pockels effect. Half-wave voltages of 15 V at 1 300 nm wavelength have been obtained. This device is probably the first integrated system showing that coherence modulation of light can be performed using integrated optics technology. This opens up new applications since it permits integration of several coherence modulators as well as several receiving interferometers to be carried out on a single chip. Bandwidths up to 6 GHz have just been demonstrated at our laboratory [26].

6.2 OPTICAL COMMUNICATIONS. — Electro-optic coherence modulators such as described above can be used to generate a sequence of optical delays larger than the coherence length with a potential bandwidth of several tens of GHz. Multiplexing experiments over several kilometer-long multimode and singlemode fibers have been conducted using multimode laser diodes and superluminescent diodes [12, 13, 15, 16]. Practically, the maximum number of channels in series topologies is estimated to be limited to about 10 by the propagation losses in the cascaded modulators (3 dB loss power per modulator) for – 50 dBm detection threshold at the detectors and a data rate of 140 Mbit/s. Very recent results have also been obtained with integrated modulators which allow 30 km long transmissions on a singlemode fiber at 400 Mbit/s [17]. An unexpected application deals with two-way transmission on a single fiber [18, 19]. In that case, coherence modulation of light is used together with conventional intensity modulation to transmit data in two directions simultaneously through one fiber and with a single light source. A bit-error-rate smaller than 10^{-10} has been demonstrated. The peculiarity of this method is that it is probably the only optical method which allows bidirectional data transmissions with identical modulation rates in the two directions. Also note that other configurations combining both series and parallel topologies can be used to increase the number of channels. Of the several possible architectures, a parallel system topology in which a single source is used to coherence-multiplex several signals for telecommunications applications was recently reported by Blair and Cormack [20] who studied the influence of the source linewidth on the system multiplexing capacity. Recently, interest has been shown in applying coherence multiplexing principles to high speed (> 10 Gbit/s) interprocessor links in parallel computers using integrated optics technology [21].

6.3 ARRAY OF SENSORS. — Interest in sensing has also grown since Al-Chalabi *et al.* [22] and Brooks *et al.* [8] pointed out that the method also applies to multiplex sensor arrays using a single source.

The sensor arrays are formed by series of unbalanced fiber Mach-Zehnder interferometers powered by a laser diode with a short coherence length relative to the path-imbalances of the sensing interferometers. The fiber Mach-Zehnder interferometers used exhibit long branches (> 10 m) in order to obtain a high sensitivity, especially for hydrophone applications in which the signals to detect may be very weak. The use of a singlemode laser source with a relatively long coherence length (> 1 m) is advantageous in that case as it facilitates more straightforward matching between the fiber Mach-Zehnder interferometer pairs forming the sensor array. However, phase-induced intensity noise which is increasingly important with increasing the coherence length limits the sensitivity of the system and can severely reduce the dynamic range of the system. A method for the reduction of this excess phase noise was proposed by Kersey and Dandridge [7], using diode laser frequency modulation to effect a frequency translation of the excess noise power. They reported an improvement of 40 dB in minimum detectable phase shift sensitivity and demonstrated a sensor with a sensitivity down to 45 μrad/ $\sqrt{\text{Hz}}$. A sensor specially designed for subnanometric measurements is described in reference [23]. Considerations on noise performance in sensing are discussed in reference [9]. Recently, a coherence-multiplexed quasi-distributed sensor based on the retardation properties of birefringent fibers has also been proposed by Turpin *et al.*, and Guresmoli *et al.* [24].

6.4 SIGNAL PROCESSING AND OPTICAL COMPUTING. — Recent work has also been directed towards the implementation of an electro-optic systolic processor, using coherence modulation principles and performing in parallel fast-matrix vector products. This type of operations play an important role in a number of signal processing applications involving FFT, digital correlations and convolutions, such as pattern recognition or radar signal processing for instance. The processor is based on the series configuration. It consists of an array of cascaded electro-optic coherence modulators in tandem with decoding modules operating as receiving interferometers. In that case, the coherence modulators are used both to multiplex data on a light beam and to compute multiplications. A description of the system is given in reference [25] which also gives the principle of operation in the case of matrix-vector products. The computing speed of the demonstrator constructed at our laboratory is currently of 50 millions of operations per second and the size of the processed matrices is 5 lines, 10^4 columns.

7. Conclusion : is the term « coherence modulation » the most appropriate ?

The point of view developed in this paper is based on models in which light is considered as stochastic fields characterized by second-order moments, i.e. coherence functions. The reasons for which the term « coherence modulation » is used are mainly based on the fact that sides lobes of coherence are generated when light propagates in a series of interferometers. This means clearly that the temporal coherence of light suffers a modulation. However the authors are often asked whether coherence modulation is the most appropriate term to describe the physical principles. Indeed another approach consists in considering the information carrier is formed physically by optical delays, rather than by the coherence degree itself. For instance, in the multiplexing schemes in figures 4 and 5, each channel corresponds to a given optical delay τ_i which behaves as an information carrier for the signal ; the latter is imprinted on light by modulating the carrier, i.e., the optical delay around the mean value τ_i. Hence the method can be termed « path-difference modulation », which is more appropriate since it gives a straightforward description of signal encoding.

An alternative point of view is also possible when noticing that an interferometer with a path-difference greater than the coherence length is equivalent to a spectral filter with a sinusoidal transmission curve. Then the series of interferometers of figure 4, as well as the receiving interferometer, can be considered as cascaded spectral filters in tandem with a receiving spectral filter whose transmission curve is tuned to select the desired channel. The method can thus be also named « spectral modulation », since many aspects are similar to the so-called wide spectrum transmission methods in signal processing. The term « coherence modulation », which rather denotes a statistical description, was first introduced by Brooks *et al.* [8] in the area of sensors, independently of previous works in the field of optical communications in which the previous considerations were used to describe the physical principles [4, 5], and is now widely used in the international optical community. All these terms are equivalent.

References

[1] See for instance BORN M., WOLF E., Principles of Optics, 6th Edition (Pergamon Press), pp. 503-505.

[2] See for instance BORN M., WOLF E., Principles of Optics, 6th Edition (Pergamon Press), pp. 364-367.

[3] FLOURNOY P. A., MCCLURE R. W., WINTJES G., White light interferometric thickness gauge, *Appl. Opt.* **11** (1972) 1907-1915.

[4] DELISLE C., CIELO P., Multiplexing in optical communications by interferometry with a large path-length difference in white light, *Canadian J. Phys.* **54** (1976) 2322-2331.

[5] GOEDGEBUER J. P., SALCEDO J., VIÉNOT J. Ch., Multiplex communication *via* electro-optic phase modulation of white light, *Optica Acta* **29** (1982) 471-477.

[6] SAKAI I., PARRY G., Multiplexing interferometric fibre sensors by frequency modulation techniques, Tech. Dig. Third Int. Conf. Optical Fiber Sensors (San Diego, Feb. 13-14, 1985) pp. 128-130.

[7] KERSEY A. D., DANDRIDGE A., Phase-noise reduction in coherence-multiplexed interferometric fibre sensors, *Electron. Lett.* **22** (1986) 616-618.

[8] BROOKS J. L., YOUNGQUIST R. C., WENTWORTH R. H., TUR M., KIM B. Y., SHAW H. J., Coherence multiplexing of fiber-optic interferometric sensors, *J. Lightwave Technol.* **3** (1985) 1062-1072.

[9] WENTWORTH R. H., Theoretical noise performance of coherence-multiplexed interferometric sensors, *J. Lightwave Technol.* **7** (1989) 941-956.

[10] GOEDGEBUER J. P., HAMEL A., PORTE H., Analysis of optical crosstalk in coherence multiplexed systems employing a short coherence laser diode with arbitrary power spectrum, *IEEE J. Quantum Electron.* **26** (1990) 1217-1226.

[11] BLOTEKJAER K. J., WENTWORTH R. H., SHAW H. J., Choosing Relative Optical Path Delays in Series-Topology Interferometric Sensor Arrays, *J. Lightwave Technol.* **5** (1987) 229-235.

[12] PORTE H., GOEDGEBUER J. P., HAMEL A., Two TV channel multimode fibre link using a single multimode laser diode and path-difference multiplexing, *Electron. Lett.* **22** (1986) 1189-1191.

[13] GOEDGEBUER J. P., PORTE H., HAMEL A., Electro-optic Modulation of multilongitudinal mode laser diodes : demonstration at 850 nm with simultaneous data transmission by coherence multiplexing, *IEEE J. Quantum Electron.* **23** (1987) 1135-1144.

[14] MOLLIER P., PORTE H., GOEDGEBUER J. P., Proton exchanged imbalanced Ti : $LiNbO_3$ Mach-Zehnder modulator, *Appl. Phys. Lett.* **60** (1992) 274-276.

[15] GOEDGEBUER J. P., FERRIÈRE R., HAMEL A., Polarization-independent transmission on a single mode fiber using coherence modulation of light, *IEEE J. Quantum Electron.* **27** (1991) 1963-1967.

[16] GOEDGEBUER J. P., HAMEL A., Coherence Multiplexing Using a Parallel Array of Electrooptic Modulators and Multimode Semiconductor Lasers, *IEEE J. Quantum Electron.* **23** (1987) 2224-2237.

[17] HAMEL A., MATHIEU M. P., PORTE H., FERRIÈRE R., GOEDGEBUER J. P., Proc. EFOC/LAN 91 (London-June 91).

[18] GOEDGEBUER J. P., HAMEL A., A novel modulation method for bidirectional transmissions on a single optical fiber, *Appl. Phys. Lett.* **57** (1990) 1384-1386.

[19] GOEDGEBUER J. P., HAMEL A., PORTE H., Full bidirectional fiber transmission using coherence-modulated lightwaves, *IEEE J. Quantum Electron.* **28** (1992) 2685-2691.

[20] BLAIR D. A., CORMACK G. D., Optimal source linewidth in a coherence multiplexed optical fiber communications system, *J. Lightwave Technol.* **10** (1992) 804-810.

[21] CHU K. W., DICKEY F. M., Optical Coherence multiplexing for interprocessor communications, *Opt. Eng.* **30** (1991) 337-344.

[22] AL-CHALABI S. A., CULSHAW B., DAVIES D. E. N., Proc. 1st International Conference on Optical Fiber Sensors (IEE) (1983) pp. 132-135.

[23] FERDINAND P., PAULET M., PILLON R., Proc. OPTO 87, Paris, May (ESI Publications, Paris) pp. 294-299.

[24] TURPIN M., BREVINGON M., ROSAS D., Proc. Congrès Mesucora, Paris, pp. 116-117 ; GURESMOLI V., VAVASSORI P., MARTINELLI M., OFS 89, Springer Proceedings in Physics **44** (Heidelberg : Springer-Verlag) pp. 513-518.

[25] GOEDGEBUER J. P., PORTE H., FERRIÈRE R., Recent advances in electro-optic coherence multiplexing, *Int. J. Optoelectron.* **6** (1991) 339-356.

[26] GUTTERIEZ C., Private communication, 1993.